Inhibition of NFAT Signaling Restores Microvascular Endothelial Function in Diabetic Mice

Garcia-Vaz, Eliana; McNeilly, Alison D; Berglund, Lisa M; Ahmad, Abrar; Gallagher, Jennifer R; Dutius Andersson, Anna-Maria

Published in:
Diabetes

DOI:
10.2337/db18-0870

Publication date:
2019

Document Version
Peer reviewed version

INHIBITION OF NFAT SIGNALING RESTORES MICROVASCULAR ENDOTHELIAL FUNCTION IN DIABETIC MICE

Journal:	*Diabetes*
Manuscript ID	DB18-0870.R3
Manuscript Type:	Original Article: Complications
Date Submitted by the Author:	26-Nov-2019
Complete List of Authors:	Garcia-Vaz, Eliana; Lund University, Clinical Sciences McNeilly, Alison; University of Dundee, Division of Clinical & Molecular Medicine; Ninewells Hospital & Medical School Berglund, Lisa M.; Lund University, Clinical Sciences Ahmad, Abrar; Lund University, Clinical Sciences Gallagher, Jennifer R; University of Dundee, Division of Clinical & Molecular Medicine; Ninewells Hospital & Medical School Dutius Andersson, Anna-Maria; Lund University, Clinical Sciences McCrimmon, Rory; University of Dundee, Division of Clinical & Molecular Medicine; Ninewells Hospital & Medical School Zetterqvist, Anna V; Lund University, Clinical Sciences Gomez, Maria; Lund University, Clinical Sciences Khan, Faisel; University of Dundee, Division of Clinical & Molecular Medicine; Ninewells Hospital & Medical School

AUTHOR ACCEPTED MANUSCRIPT VERSION OF: Garcia-Vaz, E, McNeilly, AD, Berglund, LM, Ahmad, A, Gallagher, JR, Dutius Andersson, A-M, McCrimmon, RJ, Zetterqvist, AV, Gomez, MF & Khan, F 2019, 'Inhibition of NFAT Signaling Restores Microvascular Endothelial Function in Diabetic Mice', Diabetes, vol. 68, no. 12, 180870, pp. 1-50. https://doi.org/10.2337/db18-0870

INHIBITION OF NFAT SIGNALING RESTORES MICROVASCULAR ENDOTHELIAL FUNCTION IN DIABETIC MICE

Short running title: NFAT in endothelial function

Tweet: *In vivo* inhibition of NFAT signaling restores microvascular endothelial function in diabetic mice

Eliana Garcia-Vaz[1]*, Alison D. McNeilly[2]*, Lisa M. Berglund[1], Abrar Ahmad[1], Jennifer R. Gallagher[2], Anna-Maria Dutius Andersson[1], Rory J. McCrimmon[2], Anna V. Zetterqvist[1], Maria F. Gomez[1#✉], Faisel Khan[2#✉]

[1]Department of Clinical Sciences in Malmö, Lund University Diabetes Centre, Lund University, Sweden; [2]Division of Clinical and Molecular Medicine, Ninewells Hospital & University of Dundee, Scotland

*or # indicate equal contributions

Total word count: 4723

Number of figures: 7 (+7 supplemental figures)

✉To whom correspondence should be addressed (joint correspondence):

Professor Maria F. Gomez
Dept. of Clinical Sciences, Malmö
Diabetic Complications
CRC 91:12; Box 50332
202 13 Malmö, Sweden
Phone: +46-40-391058
E-mail: maria.gomez@med.lu.se

Professor Faisel Khan
Division of Clinical and Molecular Medicine
Ninewells Hospital & Medical School
University of Dundee, DD1 9SY
Scotland, UK
Phone: +44 1382 383531
E -mail: f.khan@dundee.ac.uk

Abstract

Central to the development of diabetic macro- and microvascular disease is endothelial dysfunction, which appears well before any clinical sign, but importantly, is potentially reversible. We previously demonstrated that hyperglycemia activates NFAT in conduit and medium sized resistance arteries and that NFAT blockade abolishes diabetes-driven aggravation of atherosclerosis. Here we test whether NFAT plays a role in the development of endothelial dysfunction in diabetes.

NFAT-dependent transcriptional activity was elevated in skin microvessels of diabetic Akita (*Ins2*$^{+/-}$) mice when compared to non-diabetic littermates. Treatment of diabetic mice with the NFAT blocker A-285222 reduced NFATc3 nuclear accumulation and NFAT-luciferase transcriptional activity in skin microvessels, resulting in improved microvascular function, as assessed by laser Doppler imaging and iontophoresis of acetylcholine and localized heating. This improvement was abolished by pre-treatment with the nitric oxide synthase inhibitor L-NAME, while iontophoresis of the NO donor sodium nitroprusside eliminated the observed differences. A-285222 treatment enhanced dermis eNOS expression and plasma NO levels of diabetic mice. It also prevented induction of inflammatory cytokines IL-6 and osteopontin, lowered plasma Et-1 and blood pressure, and improved mice survival without affecting blood glucose. *In vivo* inhibition of NFAT may represent a novel therapeutic modality to preserve endothelial function in diabetes.

Introduction

Cardiovascular complications are the major cause of morbidity and mortality in patients who have diabetes. Based on current trends, the rising incidence of diabetes (expected to reach 700 million people worldwide by 2025), will undoubtedly equate to increased cardiovascular mortality. (1) Central to the development of diabetic vascular complications is endothelial dysfunction, which appears well before any clinical sign, and importantly is potentially reversible. It is a generalized phenomenon that takes place in both large blood vessels and the microvasculature. (2) Impaired endothelial function is characterized by a decreased production or bioavailability of nitric oxide (NO), leading in the larger vessels to increased vasoconstriction, inflammation and thrombosis, and predisposing to atherosclerosis; while contributing in the microvasculature to the development of retinopathy, nephropathy, cardiopathy, skin lesions and cerebrovascular dysfunction. (3) The molecular mechanisms leading to endothelial dysfunction in diabetes are still not clear.

Previous studies from our group demonstrate that hyperglycemia is an effective stimulus for activation of the calcium (Ca^{2+})/calcineurin-sensitive transcription factor Nuclear Factor of Activated T-cells (NFAT)c3 in conduit and medium-sized resistance arteries. (4-6) This activation involves the local release of extracellular nucleotides (i.e.UTP, UDP) acting on purinergic P2Y2/4 and P2Y6 receptors, leading to increased intracellular Ca^{2+} and subsequent activation of calcineurin and NFAT. (4) High glucose also reduces nuclear export of NFATc3 by inhibiting GSK-3β and JNK, contributing to increased NFATc3 nuclear accumulation. (4)

In a series of follow-up publications primarily focusing on the smooth muscle, we showed that once activated, NFAT increases the expression of inflammatory mediators in the arterial wall, such as osteopontin (OPN), cyclooxygenase-2 (COX-2), interleukin (IL)-6, vascular cell

adhesion molecule 1 (VCAM-1), tissue factor and allograft inflammatory factor-1 (AIF-1). (5-9) More recently, we demonstrated a role for NFAT in diabetes-driven atherosclerotic plaque formation via regulation of inflammatory mediators and anti-oxidant defences (i.e. NOX4 and catalase). (6; 10) However, it is still unknown whether NFAT plays a role in diabetes–driven endothelial dysfunction, particularly in microcirculatory beds where vascular complications of diabetes are commonly found. Interestingly, in cultured bovine aortic endothelial cells, blockers of calcineurin/NFAT signaling [i.e. cyclosporine A (CsA), tacrolimus (FK506)] have been shown to up-regulate endothelial NO synthase (eNOS) expression. (11). We have shown that the skin microcirculation provides a representative model of generalized microvascular function and is useful for *in vivo* experimental mechanistic studies of endothelial function in small animals. (12; 13).

In this paper we hypothesize that NFAT is expressed in skin microvessels, that hyperglycemia may activate NFAT in skin microvessels and that *in vivo* blockade of NFAT with A-285222 can attenuate microvascular dysfunction in diabetic mice. We also explore whether eNOS expression may be modulated by NFAT-signaling in this context.

Research Design and Methods

An expanded version of this section is available in the Online Data Supplement. Adult male diabetic Akita (*Ins2*$^{+/-}$) mice were used according to the study protocol shown in **Figure 1A**, as well as crossbred with FVBN 9x-NFAT-luciferase reporter (NFAT-luc) mice (4; 14; 15) to generate Akita/NFAT-luc mice and non-diabetic wild-type (WT)/NFAT-luc littermates. Akita mice have a point mutation of the insulin 2 gene which leads to pancreatic beta-cell apoptosis, hypoinsulinemia and severe hyperglycemia. Non-obese, Akita mice develop type 2 diabetes phenotypes including peripheral and hepatic insulin resistance and cardiac remodeling and as such are a good model for studying vascular complications of type 1 and lean type 2 diabetes subjects.(16) Microvascular function was assessed non-invasively and longitudinally using a laser Doppler imager in combination with iontophoresis of endothelium-dependent and –independent vasodilators [acetylcholine (ACh) and sodium nitroprusside (SNP), respectively] and localized heating as previously described. (12; 13) To standardize basal perfusion, blood vessels were pre-constricted with iontophoresis of 1% phenylephrine (PE) for 5 min (current=100 μA), prior iontophoresis of ACh or SNP. To determine the contribution of endothelium-derived NO to ACh-mediated vasodilatation, microvascular responses to ACh were assessed 30 min after i.p. injection of the non-selective inhibitor of NO synthase, N(G)-nitro-L-arginine methyl ester (L-NAME, Sigma Chemicals; 20 mg/kg). (12) On a separate day and to determine the maximum microvascular dilator capacity, a hyperemic response was initiated by localized heating of the skin using a specially designed heating probe (SH02™ skin heating unit and SHP3 probe, Moor Instruments Ltd, Axminster, UK). Perfusion was measured continuously as the temperature of the heating probe was increased to 42°C (1°C/min) and maintained for >10 min, which was sufficient for maximum vasodilatation to plateau.

Mice were euthanized by cervical dislocation after anesthesia with 3% isoflurane in oxygen (2 L/min) or for NFAT-luc experiments, anaesthetized by intraperitoneal (i.p.) injection of 7.5 mg ketamine hydrochloride and 2.5 mg xylazine per 100 g body weight and euthanized by exsanguination through cardiac puncture. All animal protocols were performed in accordance with UK Home Office regulations (Project License PIL60/4265) and the Malmö/Lund Animal Care and Use Committee (Permits M78-10, M29-12, and M9-15) and abided by the Guide for the Care and Use of Laboratory Animals published by the Directive 2010/63/EU of the European Parliament. Luciferase activity was measured in the skin, aortic arch, abdominal aorta and carotid arteries in tissue homogenates as previously described. (14) Skin sections were used for histology (hematoxylin and eosin; H&E), for immunohistochemistry (eNOS) or for quantification of NFATc3 nuclear accumulation using confocal microscopy as previously described. (14; 17; 18) Organ culture of skin biopsies and dissociation of dermis and epidermis was done according to established protocols. (19-22) Skin fractions were used for gene expression, absolute quantification of NFAT isoforms and western blot analysis. Plasma cytokines, endothelial activation markers and total NO were measured in blood samples taken from the tail vein; albumin and creatinine were measured from urine. Total NO related species (nitrite, nitrate, nitrosothiols) were measured 4 weeks after treatment with A-285222 (Post-2) using a gas phase chemiluminescence reaction of NO with ozone using Sievers nitric oxide analyzer (NOA) model 280i (Analytix, Bodon, UK). Blood pressure was assessed using a non-invasive tail-cuff blood pressure system. A-285222 inhibits all NFAT family members and was kindly provided by Abbott Laboratories (Abbott Park, IL). This drug belongs to a series of 3,5-bis (trifluoromethyl)pyrazole (BTP) derivatives demonstrated to maintain NFAT in a phosphorylated state, blocking its nuclear import and subsequent transcription, without affecting NF-kB or AP-1 activation, or calcineurin phosphatase activity (23). Results are expressed as means ± SEM unless specified otherwise.

Results

In vivo treatment with A-285222 improves skin microvascular responses to acetylcholine and localized heating in diabetic mice

While no significant differences in the responses to phenylephrine (PE) at baseline were found between non-diabetic WT and Akita mice, microvascular responses to iontophoresis of ACh were impaired in Akita mice (**Figure 1B**), with less vasodilation to ACh than in non-diabetic WT mice. Diabetic Akita mice were treated with the NFAT blocker A-285222 (0.29 mg/kg body weight) or vehicle (saline) for 4 weeks and microvascular function was assessed before ("Pre"; **Figure 1C**), directly after ("Post-1"; **Figure 1D**) or 4 weeks after the end of the treatment ("Post-2"; **Figure 1E**). Before commencement of treatment, baseline measurements of microvascular function were not significantly different between the groups (**Figure 1C**). Treatment with A-285222 resulted in improved ACh responses compared with vehicle treated controls at both time-points post-treatment (**Figure 1D-E**). **Figure 1F** summarizes maximum responses to ACh at each time-point showing a loss of endothelial function in Akita mice that is not observed in mice treated with A-285222. Treatment had no effect on blood glucose or body weight (**Figures 1G-H**).

Pre-treatment with the NO synthase inhibitor N(G)-nitro-L-arginine methyl ester (L-NAME) 30 min prior to iontophoresis of ACh completely abrogated the improved response observed after treatment with A-285222, and had no impact on the responses measured in vehicle-treated mice (**Figure 2A**). The dotted line in **Figure 2A** indicates the ACh response in mice after treatment with A-285222 in the absence of L-NAME treatment (corresponding to "Post-1" data in **Figure 1F**). Iontophoresis of the NO donor SNP on the other hand, eliminated the

differences in microvascular responses observed after treatment between the groups, effectively vasodilating the vessels of vehicle treated mice to the same extent as those that had been treated with A-285222 (**Figure 2B**). Treatment with A-285222 had no effect on skin microvascular responses to ACh (regardless whether animals were treated or not with L-NAME prior iontophoresis of ACh), and no effect on the responses to SNP on blood glucose levels or body weight in control non-diabetic wild-type mice (**Supplemental figures 1 and 2A-B**). No significant differences were found in the responses to PE in WT and Akita mice with and without A285222 (not shown).

Skin microvascular responses to localized heating, which are largely dependent on NO, (24)were comparable between NFAT and saline-treated groups when measured prior to initiating the treatment (**Figure 2C**). Four weeks' treatment with the NFAT blocker A-285222 resulted in an improved vasodilator response compared with vehicle-treated mice (**Figures 2D-E**). The longitudinal change in maximum vasodilator response (Pre to Post-1) indicates a loss of heat-induced vasodilation in vehicle-treated diabetic mice over 4 weeks (negative delta value), whereas A-285222 treatment improves the vasodilator response to heat (positive delta value), such that the difference between the groups was significantly different (**Figure 2F**). Treatment with the NFAT blocker A-285222 had no effect on skin microvascular responses to localized heating in control non-diabetic wild-type mice (**Supplemental figure 2C-F**).

NFATc3 is the predominant NFAT isoform expressed in mouse skin

To investigate NFAT isoforms expressed in mouse skin and in particular in skin microvessels, we collected skin from the flank of the mice corresponding to the area used for microvascular endothelial function measurements (**Figure 3A**). Since vessels in the mouse skin are predominantly located in the dermis (arrowheads in **Figure 3B**), we enzymatically dissociated

the dermis from the epidermis for measurements of NFAT isoform expression and NFAT-dependent transcriptional activity. Absolute quantification of NFAT isoform mRNA expression showed that NFATc3 is the predominant isoform in both skin fractions (**Figure 3C**), followed by NFATc1, NFATc2 and NFATc4 which were expressed at 6-, 17- and 630-fold lower copy number in dermis when compared to NFATc3. A tendency towards lower NFAT isoform expression was observed in the dermis of Akita mice when compared to control WT mice, but differences were only statistically significant for NFATc4, which is overall expressed at very low levels (**Figure 3D**). Using confocal immunofluorescence microscopy of skin whole mounts, we found abundant NFATc3 staining in microvascular endothelial cells, visualized by CD31 positive immunostaining (**Figure 3E**). Despite comparable NFAT mRNA levels in dermis and epidermis, the dermis accounted for most of the NFAT-dependent transcriptional activity measured in whole skin samples (**Figure 3F**). Treatment with dispase causes separation at the dermal-epidermal basement membrane, (21) yielding pure fractions as evidenced by exclusive expression of the endothelial cell marker CD31 in the dermis fraction in western blot experiments (**Figure 3G**).

***In vivo* treatment with A-285222 blocks diabetes-induced NFAT activation in the dermis**

In samples collected at termination ("Post-2") from the same mice used for measurements of microvascular function, we found that *in vivo* treatment with A-285222 significantly decreased NFATc3 nuclear accumulation in skin microvessels (**Figures 4A-B**). NFAT-dependent transcriptional activity in the skin of Akita mice gradually increased with longer durations of high glucose exposure (**Supplemental figure 3A**). Akita/NFAT-luc mice develop pronounced and sustained hyperglycemia from 4 weeks postnatal, failing to gain as much body weight as WT/NFAT-luc littermates, as well as proteinuria from 8 weeks postnatal and further increasing as the mice became older (**Supplemental figures 3B-D**).

In a separate cohort from that used for monitoring time-dependent effects of diabetes in the model (**Supplemental figure 3**), Akita/NFAT-luc and WT/NFAT-luc littermates were treated with A-285222 (0.29 mg/kg body weight) or vehicle (saline) for 4 weeks and NFAT-dependent transcriptional activity was determined in skin and various arteries. In intact whole skin, a tendency to increased NFAT-luciferase activity (p=0.06) was observed in Akita/NFAT-luc mice when compared to non-diabetic WT/NFAT-luc mice, while activity was lower in diabetic mice treated with A-285222 (**Figure 4C**). Further analysis of the dermis fraction, where vessels are located, showed a significant diabetes-induced increase in luciferase mRNA, which was completely blocked by treatment with A-285222 (**Figure 4D**). The effect of the blocker is unlikely due to effects on glucose metabolism, since neither blood glucose nor body weight were affected by the treatment (**Supplemental Figure 4A-B**). In line with previous work from our lab in which a streptozotocin-induced diabetes model was used (5; 6), NFAT-luciferase activity was significantly enhanced in the aortic arch of Akita/NFAT-luc mice when compared to WT/NFAT-luc controls, and it was completely abolished by A-285222 (**Supplemental figure 4C**). A similar pattern was observed in the abdominal aorta and carotid arteries (**Supplemental figures 4D-E**). No effects of the treatment were observed in the non-diabetic mice (**Figures 4C-D; Supplemental figures 4C-D**).

***In vivo* inhibition of NFAT with A-285222 enhances eNOS expression and plasma NO levels**

To elucidate the mechanism underlying the effects of NFAT signaling inhibition on microvascular function, we measured eNOS expression in the dermis of Akita/NFAT-luc and WT/NFAT-luc mice after treatment with A-285222 or vehicle. Although we could not detect

diabetes-driven changes in eNOS expression at the mRNA level (**Figure 5A**), both eNOS and p-eNOS protein expression were lower in Akita mice compared to non-diabetic WT mice (**Figure 5B**). Interestingly, a clear upregulation of eNOS mRNA expression was observed in diabetic mice directly after treatment with A-285222. Although not significant, eNOS mRNA seemed to remain elevated at 9 weeks after the end of the treatment (**Figure 5A**), but no significant changes were detected at the protein level (**Figure 5B**). Consistent with the elevated eNOS mRNA levels in the dermis, higher circulating levels of NO were found after treatment with A-285222 ("Post-2") in the same Akita mice that exhibited improved endothelial function, when compared with vehicle-treated Akita mice (**Figure 5C**). Immunohistochemistry confirmed expression of eNOS protein in the wall of skin microvessels in these mice (**Figure 5D**).

To assess whether the effects on NFAT-transcriptional activity and eNOS expression induced by systemically administered A-285222 could be attributed, at least in part, to local effects of the blocker on the skin, we organ cultured intact skin samples from NFAT-luc mice using a protocol that has been shown to preserve both skin function and structure. (19) Culture of the skin with A-285222 (1 μmol/L) for 24 hours resulted in significantly reduced luciferase mRNA and a concomitant increase in eNOS mRNA expression measured in the dermis fractions (**Figures 5E-F**). Organ culture of the skin had per se an impact on eNOS and p-eNOS expression in the dermis, with significantly increased expression levels at 24 hours of culture, but levels no different from those measured in freshly dissociated dermis at 48 hours (**Supplemental figure 5**). At 48 hours, eNOS protein expression was significantly higher in samples that had been cultured with A-285222 compared to controls, while no significant changes were found in p-eNOS protein expression (**Figure 5G**). ***In vivo*** **inhibition of NFAT**

prevents the induction of inflammatory cytokines, lowers plasma endothelin-1 (Et-1) and blood pressure and improves survival of diabetic mice

The improved microvascular responses to ACh and localized heat observed in Akita mice after treatment with A-285222 were accompanied by significantly reduced plasma levels of the pro-inflammatory cytokines IL-6, OPN and the endothelial activation marker soluble intercellular adhesion molecule 1 (sICAM) directly after the intervention ("Post-1"), while other cytokines or markers (e.g. IL-1α, IL-10, E-selectin) were unaffected (**Figure 6A-F**). The inhibitory effect of the blocker on IL-6 and OPN remained evident 4 weeks after the intervention ("Post-2"). Except IL-1α, all other plasma molecules increased during the study protocol in the vehicle treated mice as they aged (**Figures 6A-F**). Despite elevated levels of circulating IL-6 and OPN, we could not detect changes in the levels of IL-6 or OPN mRNA in the dermis of diabetic or WT mice treated with A-285222 (**Supplemental figure 6**)

In addition to increased levels of circulating NO (**Figure 5C**), plasma Et-1 was significantly reduced 4 weeks after treatment with A-285222 when compared to levels in vehicle treated Akita mice (**Figure 7A**). At the same time point, both systolic and diastolic blood pressure was significantly lower in A-285222 treated Akita mice compared with vehicle treated mice (**Figure 7B-C**). There was no significant difference in heart rate between groups (445±51 vs. 424±43 beats per minute vehicle vs. A-285222, p=0.767). Treatment with the NFAT blocker A-285222 had no effect on plasma levels of inflammatory cytokines or Et-1 in control non-diabetic wild-type mice (**Supplemental figure 7**).

As the study progressed, many of the Akita mice appeared ill and ~40% either died or had to be euthanized before completion of the study because of failure to thrive (**Figure 7D**). Even though Kaplan-Meier curves were not statistically different between the two groups, all mice

treated with A-285222 survived until termination of the study (**Figure 7D**, p=0.0817). **Figure 7E** shows survival data from an independent study conducted for another project, which included 33 Akita mice (C57BL/6J background; mixed genders) that were treated with A-285222 or vehicle for 4 weeks as in this current study. In line with the data in **Figure 7D**, all A-285222 treated mice survived until termination of the study, whereas a substantial number of vehicle treated mice died or had to be euthanized (**Figure 7E**). Differences between survival curves were statistically significant (**Figure 7E**, p=0.0299) and remained significant even if only male mice are included in the analysis (p=0.0085; N=16).

Discussion

The findings from the present *in vivo* study show that diabetes is associated with an increase in NFAT-dependent transcriptional activity and microvascular dysfunction which can be significantly improved by blocking of NFAT activation. The improvement in microvascular responses was associated with a reduction in vascular NFATc3 nuclear accumulation and NFAT-dependent transcriptional activity in the skin and it was mediated largely through increased NO availability. Our results point at the NFAT signaling as a novel pathway involved in the development of microvascular dysfunction in diabetes. Blocking of hyperglycemia-induced NFAT transcriptional activity with A-285222 leads to an improvement in microvascular function which in combination with the observed reduction in circulating pro-inflammatory cytokines and Et-1 levels may contribute to lower blood pressure and increased survival of the mice.

We believe our findings of improvements in the skin microcirculation following blocking of NFAT activation have clinical significance. Measurement of skin microvascular responses to iontophoresis of ACh and localized heating using laser Doppler imaging has proven a successful strategy to monitor and predict diabetic complications in clinical studies. Skin microvascular function is significantly impaired in patients with diabetic retinopathy compared to those without complications (25; 26) and in young children with diabetes before clinical signs of microangiopathy. (27) Furthermore, skin microvascular responses are strongly correlated to insulin sensitivity, coronary heart disease and its risk factors. (28)

Role of NFAT in Skin Microvascular Dysfunction

Most NFAT-related studies in the context of skin have focused on the role of NFATc2 in epidermal keratinocytes in skin diseases such as psoriasis. (29-31) The absolute

quantification experiments unexpectedly revealed that NFATc3 is the predominant NFAT-isoform in both dermis and epidermis (**Figure 3C**). This is interesting considering that NFATc3 seems to be the dominant NFAT isoform in all other vascular beds that we have examined so far, including cerebral, retinal, carotid, aorta, hepatic, renal, femoral, mesenteric arteries and portal vein (unpublished results and (14; 18; 32)) also, considering that NFATc3 is readily activated by elevated extracellular glucose. (4-6; 32)

The predominance of this particular NFATc3 isoform in the dermis, where the microvessels are mainly located and the increased NFAT-transcriptional activity observed in the Akita mice, suggest that NFAT activation could be contributing to the observed deterioration in microvascular responses. Worth noting though is that differences in baseline microvascular responses to ACh between WT and diabetic mice were noticeable already at 7-12 weeks of age, while we could only dissect the difference in whole skin NFAT-luciferase activity beyond 12 weeks of age. This could be due to limitations of the technique when using whole-skin homogenates compared to the better resolution obtained when using isolated dermis (please see comparison between **Figures 4C** and **D**), but also most likely due to engagement of other hyperglycemia-induced factors recognized as drivers of endothelial dysfunction early on in the process, perhaps increased oxidative stress (33; 34) and inflammation. (35)

Despite potentially multiple pathways driving the deterioration in microvascular responses in the diabetic mice, we found a clear improvement in skin microvascular function after inhibition of NFAT signaling with A-285222. Treatment effects could be attributed to changes in NFAT activity as demonstrated by the reduction in NFATc3 nuclear accumulation in skin microvessels and by reduced NFAT-dependent transcriptional activity, as assessed by NFAT-luciferase activity and luciferase mRNA expression in the dermis. Importantly, the

decreased NFAT activation and improved microvascular function were not due to a glucose lowering effect of the NFAT blocker.

Role of NO in the improved Microvascular Responses after NFAT inhibition

In agreement with our previous findings demonstrating that the skin microvascular response to iontophoresis of ACh in mice is mediated through NO, (12) we show here that the improvement in microvascular responses to ACh immediately following 4 weeks' inhibition of NFAT with A-285222 and maintained for 4 weeks after the end of treatment, is due to enhanced production of NO in the diabetic mice compared with vehicle treated mice. This was evidenced by abrogation of the improved microvascular response following inhibition of NO production by L-NAME. The improvement in microvascular responses to ACh comes from endothelium-derived NO and not from a generalized improvement in smooth muscle responsiveness. Further support for increased NO bioavailability after treatment with A-285222, comes from the finding of improved sustained maximum vasodilator response to localized heating, which is largely mediated through an NO-dependent pathway. (24) In addition to a significant decrease in NFAT activation in the dermis of diabetic mice after treatment with A-285222, as evidenced by decreased luciferase mRNA, we found significant upregulation of eNOS expression, which further supports the role of NFAT signaling in mediating microvascular responses via increased NO bioavailability. Collectively, these data suggest that inhibition of NFAT with A-285222 leads to enhanced NO bioavailability in the skin of Akita mice, rather than affecting the downstream smooth muscle response to NO.

While our data supports the idea that inhibition of NFAT-transcriptional activity increases NO bioavailability in the skin microvasculature and while positive eNOS immunostaining was found in skin microvessels, we cannot exclude the possibility of A-285222 affecting other

potential NO producing cells in the skin. Mowbray et al (36) demonstrated the presence of enzyme-dependent NO production in all cell types of human skin, including keratinocytes, melanocytes and immune cells but did not attribute storage site to any particular cell.

Treatment with A-285222 was also associated with significantly elevated plasma NO in diabetic mice, which raises the question of whether the improved microvascular response was the result of systemic or local effects of the drug on the skin. While our findings cannot exclude systemic effects (discussed in the next section), the organ culture experiments showing significantly decreased NFAT-dependent transcriptional activity and concomitantly increased eNOS mRNA and protein expression in the dermis after overnight culture of whole skin with A-285222 certainly support the idea that at least part of the improved microvascular function observed *in vivo* could be attributed to local effects of the drug on NFAT activity in the skin. We did not observe any effects of NFAT inhibition on the levels of p-eNOS, suggesting a regulatory role in the expression but not the activity of eNOS.

Our findings are at odds with findings from other studies. Yang et al reported vascular endothelial growth factor (VEGF)-induced activation of calcineurin/NFAT signaling in endothelial progenitor cells (EPCs), which lead to increased eNOS protein expression and NO production, while inhibition of calcineurin with cyclosporine A or inhibition of NFAT with 11R-VIVIT decreased eNOS protein levels and NO production. (37) This discrepancy could be due to cell specific differences between circulating EPCs (obtained by culture of mononuclear cells from human peripheral blood) and microvascular cells *in situ* regarding the NFAT isoform engaged in the regulation of NO (NFATc1 in theirstudy), or differences in the transcriptional program engaged by the different stimuli (VEGF vs hyperglycemia in our study) or combinations thereof. We and others have previously demonstrated that NFAT

isoforms co-expressed in the same cell type can be differentially regulated by the same stimuli and that much of what determines the efficiency of the stimulus is the ability to deliver an appropriate pattern of intracellular calcium signaling in combination with precise regulation of NFAT export kinases (17; 38-40). In pancreatic acinar cells for example, we showed that NFATc3 but not NFATc1 is readily activated by cholecystokinin or by ACh. (41) Another example of differential control of NFAT isoforms is illustrated by the dramatic NFATc3 activation in the endothelium of retinal microvessels after acute hyperglycemia and the complete lack of NFATc2 response to elevated extracellular glucose in retinal endothelial cells. (32) Our data cannot rule out that the effects of A-285222 on microvascular function can be mediated by the other NFATc isoforms, despite NFATc3 being the predominant isoform in this preparation and one readily inhibited by treatment with A-285222.

In another elegant study demonstrating the importance of inositol 1,4,5-triphosphate receptor 1(IP3R1) for activation of eNOS in endothelial cells and maintenance of blood pressure, Yuan et al proposed that the increased eNOS expression and phosphorylation downstream the IP3R1 is mediated via calcineurin/NFATc3 signaling. (42) While they provide solid evidence for the involvement of IP3R1 in eNOS activation, the involvement of NFATc3 is less well-supported. Conclusions are based on confocal microscopy measurements of NFATc3 nuclear accumulation in a limited number of HUVEC cells, a cell-type of questionable relevance for blood pressure control, without further confirmation of changed NFAT-dependent transcriptional activity as a consequence of the nuclear translocation. Because calcineurin not only interacts with NFAT but also with a large number of substrates, (43) calcineurin inhibitors (i.e. CsA used by Yuan et al, and FK506) are ambiguous tools for dissecting the potential involvement of NFAT signaling. Instead, the A-285222 compound used here has

been shown to maintain NFAT in a phosphorylated state without affecting calcineurin phosphatase activity. (23)

The Role of NFAT and eNOS in the skin in Blood Pressure Regulation

Our findings in the skin have potential translational importance to the regulation of blood pressure. The skin can be considered as one of the largest organs in the body and by virtue of its large NO storage capacity, the potential for regulation of blood pressure by the skin microcirculation has come under recent interest. (44) Indeed, our data would support such an idea since changes in NFAT-transcriptional activity and eNOS expression after treatment with A-285222 were associated with a significant reduction in blood pressure, although it is also possible that the blood pressure lowering effects of NFAT blocking could arise from changes in vascular function in areas other than the skin or in combination with changes in the skin. Santana et al have demonstrated a role of NFATc3 in mediating angiotensin II-induced hypertension via down-regulation of the beta1 subunit of large conductance, calcium-activated K^+ channels and Kv1.2 channels in arterial smooth muscle. (45; 46) Interestingly, treatment with A-285222 resulted not only in increased eNOS expression in the skin but also in elevated circulating NO levels. This is in line with what others have shown, namely that serum total NO-related products correlate directly with those of the upper dermis. (47)

Even though the organ culture experiments support the idea of a local direct effect of A-285222 on NFAT activity and eNOS production, it is possible that parallel systemic effects of the blocker or local effects elsewhere than in the skin could lead to changes in circulating molecules which are capable of affecting microvascular function and blood pressure. We did indeed measure an effect of A-285222 treatment on plasma levels of inflammatory cytokines and Et-1.

In conclusion, we have shown in this *in vivo* study, with the advantage of longitudinal measurements of microvascular function at different time points in the same animals that hyperglycemia-induced NFAT activation is associated with endothelial dysfunction in the microcirculation, which can be markedly improved by therapeutic blocking of NFAT activation. The improvement in endothelial function is largely mediated through increased availability of NO and this, combined with a more anti-inflammatory phenotype and reduction in blood pressure, might underlie the increased survival of A-285222-treated mice. Further studies should explore the potential of NFAT inhibition as a novel therapeutic modality for the treatment of diabetic microvascular dysfunction.

Acknowledgements

We thank Dr. Anna Zetterqvist, Dept of Clinical Sciences, Lund University, Sweden, for valuable discussions.

Funding: This work was supported by the British Heart Foundation (Project Grant # PG/12/58/29767), The Swedish Heart and Lung Foundation [#20160872]; the Swedish Research Council [#2018-02837; #2014-03352; EXODIAB #2009-1039], the Swedish Society for Medical Research, the Swedish Foundation for Strategic Research (LUDC-IRC #15-0067), The Swedish Diabetes Association (Diabetesfonden), the Crafoord, Albert Påhlsson and Knut & Alice Wallenberg foundations. Also by Innovative Medicines Initiative Joint Undertaking SUMMIT [#115006], comprising funds from the European Union's Seventh Framework Programme [FP7/2007-2013] and EFPIA companies' in kind contribution.

Author contributions: EGV, ADM, LMB, AA, JRG, AMDA and AVZ performed the experimental work. All authors contributed to the design of the study, the analysis and interpretation of the data and the writing of the manuscript. MFG, FK and RJM secured funding for the study. MFG and FK conceived, supervised all parts of the study and wrote the article. All authors critically revised and approved the final version of this article.

M.F.G. and F.K. are the guarantors of this work and, as such, had full access to all the data in the study and take responsibility of the data and the accuracy of the data analysis.

Duality of Interest: No potential conflicts of interest relevant to this article were reported.

References

1. Worldwide trends in diabetes since 1980: a pooled analysis of 751 population-based studies with 4.4 million participants. The Lancet 2016;387:1513-1530
2. Shi Y, Vanhoutte PM: Macro- and Microvascular Endothelial Dysfunction in Diabetes. Journal of Diabetes 2017:n/a-n/a
3. Gimbrone MA, García-Cardeña G: Endothelial Cell Dysfunction and the Pathobiology of Atherosclerosis. Circulation research 2016;118:620-636
4. Nilsson J, Nilsson LM, Chen Y-W, Molkentin JD, Erlinge D, Gomez MF: High Glucose Activates Nuclear Factor of Activated T Cells in Native Vascular Smooth Muscle. Arteriosclerosis, thrombosis, and vascular biology 2006;26:794-800
5. Nilsson-Berglund LM, Zetterqvist AV, Nilsson-Ohman J, Sigvardsson M, Gonzalez Bosc LV, Smith ML, Salehi A, Agardh E, Fredrikson GN, Agardh CD, Nilsson J, Wamhoff BR, Hultgardh-Nilsson A, Gomez MF: Nuclear factor of activated T cells regulates osteopontin expression in arterial smooth muscle in response to diabetes-induced hyperglycemia. Arteriosclerosis, thrombosis, and vascular biology 2010;30:218-224
6. Zetterqvist AV, Berglund LM, Blanco F, Garcia-Vaz E, Wigren M, Duner P, Andersson AM, To F, Spegel P, Nilsson J, Bengtsson E, Gomez MF: Inhibition of nuclear factor of activated T-cells (NFAT) suppresses accelerated atherosclerosis in diabetic mice. PloS one 2013;8:e65020
7. Orr AW, Lee MY, Lemmon JA, Yurdagul A, Jr., Gomez MF, Schoppee Bortz PD, Wamhoff BR: Molecular Mechanisms of Collagen Isotype-Specific Modulation of Smooth Muscle Cell Phenotype. Arteriosclerosis, thrombosis, and vascular biology 2008;29:225-231
8. Lee MY, Garvey SM, Baras AS, Lemmon JA, Gomez MF, Schoppee Bortz PD, Daum G, LeBoeuf RC, Wamhoff BR: Integrative genomics identifies DSCR1 (RCAN1) as a novel NFAT-dependent mediator of phenotypic modulation in vascular smooth muscle cells. Hum Mol Genet 2010;19:468-479
9. Berglund LM, Kotova O, Osmark P, Grufman H, Xing C, Lydrup ML, Goncalves I, Autieri MV, Gomez MF: NFAT regulates the expression of AIF-1 and IRT-1: yin and yang splice variants of neointima formation and atherosclerosis. Cardiovascular research 2012;93:414-423
10. Blanco F, Heinonen SE, Gurzeler E, Berglund LM, Dutius Andersson AM, Kotova O, Jonsson-Rylander AC, Yla-Herttuala S, Gomez MF: In vivo inhibition of nuclear factor of activated T-cells leads to atherosclerotic plaque regression in IGF-II/LDLR(-/-)ApoB(100/100) mice. Diabetes & vascular disease research 2018:1479164118759220
11. Navarro-Antolin J, Hernandez-Perera O, Lopez-Ongil S, Rodriguez-Puyol M, Rodriguez-Puyol D, Lamas S: CsA and FK506 up-regulate eNOS expression: role of reactive oxygen species and AP-1. Kidney international Supplement 1998;68:S20-24
12. Belch JJ, Akbar N, Alapati V, Petrie J, Arthur S, Khan F: Longitudinal assessment of endothelial function in the microvasculature of mice in-vivo. Microvascular research 2013;85:86-92
13. Akbar N, Nanda S, Belch J, Cohen P, Khan F: An important role for A20-binding inhibitor of nuclear factor-kB-1 (ABIN1) in inflammation-mediated endothelial dysfunction: an in vivo study in ABIN1 (D485N) mice. Arthritis research & therapy 2015;17:22
14. Nilsson LM, Sun ZW, Nilsson J, Nordstrom I, Chen YW, Molkentin JD, Wide-Swensson D, Hellstrand P, Lydrup ML, Gomez MF: Novel blocker of NFAT activation inhibits IL-6 production in human myometrial arteries and reduces vascular smooth muscle cell proliferation. American journal of physiology Cell physiology 2007;292:C1167-1178
15. Wilkins BJ, Dai YS, Bueno OF, Parsons SA, Xu J, Plank DM, Jones F, Kimball TR, Molkentin JD: Calcineurin/NFAT coupling participates in pathological, but not physiological, cardiac hypertrophy. Circulation research 2004;94:110-118
16. Hong EG, Jung DY, Ko HJ, Zhang Z, Ma Z, Jun JY, Kim JH, Sumner AD, Vary TC, Gardner TW, Bronson SK, Kim JK: Nonobese, insulin-deficient Ins2Akita mice develop type 2 diabetes phenotypes including insulin resistance and cardiac remodeling. American journal of physiology Endocrinology and metabolism 2007;293:E1687-1696
17. Stevenson AS, Gomez MF, Hill-Eubanks DC, Nelson MT: NFAT4 movement in native smooth muscle. A role for differential Ca(2+) signaling. The Journal of biological chemistry 2001;276:15018-15024

18. Gomez MF, Stevenson AS, Bonev AD, Hill-Eubanks DC, Nelson MT: Opposing actions of inositol 1,4,5-trisphosphate and ryanodine receptors on nuclear factor of activated T-cells regulation in smooth muscle. The Journal of biological chemistry 2002;277:37756-37764
19. Varani J: Preservation of human skin structure and function in organ culture. Histology and histopathology 1998;13:775-783
20. Varani J, Perone P, Merfert MG, Moon SE, Larkin D, Stevens MJ: All-trans retinoic acid improves structure and function of diabetic rat skin in organ culture. Diabetes 2002;51:3510-3516
21. Hybbinette S, Bostrom M, Lindberg K: Enzymatic dissociation of keratinocytes from human skin biopsies for in vitro cell propagation. Experimental dermatology 1999;8:30-38
22. Stenn KS, Link R, Moellmann G, Madri J, Kuklinska E: Dispase, a neutral protease from Bacillus polymyxa, is a powerful fibronectinase and type IV collagenase. The Journal of investigative dermatology 1989;93:287-290
23. Trevillyan JM, Chiou XG, Chen YW, Ballaron SJ, Sheets MP, Smith ML, Wiedeman PE, Warrior U, Wilkins J, Gubbins EJ, Gagne GD, Fagerland J, Carter GW, Luly JR, Mollison KW, Djuric SW: Potent inhibition of NFAT activation and T cell cytokine production by novel low molecular weight pyrazole compounds. The Journal of biological chemistry 2001;276:48118-48126
24. Johnson JM, Kellogg DL: Local thermal control of the human cutaneous circulation. Journal of applied physiology 2010;109:1229-1238
25. Tooke JE, Ostergren J, Lins PE, Fagrell B: Skin microvascular blood flow control in long duration diabetics with and without complications. Diabetes Res 1987;5:189-192
26. Wilson SB, Jennings PE, Belch JJ: Detection of microvascular impairment in type I diabetics by laser Doppler flowmetry. Clin Physiol 1992;12:195-208
27. Khan F, Elhadd TA, Greene SA, Belch JJ: Impaired skin microvascular function in children, adolescents, and young adults with type 1 diabetes. Diabetes care 2000;23:215-220
28. RG IJ, de Jongh RT, Beijk MA, van Weissenbruch MM, Delemarre-van de Waal HA, Serne EH, Stehouwer CD: Individuals at increased coronary heart disease risk are characterized by an impaired microvascular function in skin. European journal of clinical investigation 2003;33:536-542
29. Al-Daraji WI, Grant KR, Ryan K, Saxton A, Reynolds NJ: Localization of Calcineurin/NFAT in Human Skin and Psoriasis and Inhibition of Calcineurin/NFAT Activation in Human Keratinocytes by Cyclosporin A. Journal of Investigative Dermatology 2002;118:779-788
30. Reynolds NJ, Al-Daraji WI: Calcineurin inhibitors and sirolimus: mechanisms of action and applications in dermatology. Clinical & Experimental Dermatology 2002;27:555-561
31. Brun C, Demeaux A, Guaddachi F, Jean-Louis F, Oddos T, Bagot M, Bensussan A, Jauliac S, Michel L: T-Plastin Expression Downstream to the Calcineurin/NFAT Pathway Is Involved in Keratinocyte Migration. PloS one 2014;9:e104700
32. Zetterqvist AV, Blanco F, Öhman J, Kotova O, Berglund LM, de Frutos Garcia S, Al-Naemi R, Wigren M, McGuire PG, Gonzalez Bosc LV, Gomez MF: Nuclear Factor of Activated T Cells Is Activated in the Endothelium of Retinal Microvessels in Diabetic Mice. Journal of diabetes research 2015;2015:14
33. Tabit CE, Chung WB, Hamburg NM, Vita JA: Endothelial dysfunction in diabetes mellitus: molecular mechanisms and clinical implications. Reviews in endocrine & metabolic disorders 2010;11:61-74
34. Tesfamariam B, Cohen RA: Free radicals mediate endothelial cell dysfunction caused by elevated glucose. American Journal of Physiology - Heart and Circulatory Physiology 1992;263:H321-H326
35. Goldberg RB: Cytokine and cytokine-like inflammation markers, endothelial dysfunction, and imbalanced coagulation in development of diabetes and its complications. The Journal of clinical endocrinology and metabolism 2009;94:3171-3182
36. Mowbray M, McLintock S, Weerakoon R, Lomatschinsky N, Jones S, Rossi AG, Weller RB: Enzyme-independent NO stores in human skin: quantification and influence of UV radiation. The Journal of investigative dermatology 2009;129:834-842
37. Yang L, Guan H, He J, Zeng L, Yuan Z, Xu M, Zhang W, Wu X, Guan J: VEGF increases the proliferative capacity and eNOS/NO levels of endothelial progenitor cells through the calcineurin/NFAT signalling pathway. Cell biology international 2012;36:21-27

38. Sumit M, Neubig RR, Takayama S, Linderman JJ: Band-pass processing in a GPCR signaling pathway selects for NFAT transcription factor activation. Integrative biology : quantitative biosciences from nano to macro 2015;7:1378-1386
39. Tomida T, Hirose K, Takizawa A, Shibasaki F, Iino M: NFAT functions as a working memory of Ca2+ signals in decoding Ca2+ oscillation. The EMBO journal 2003;22:3825-3832
40. Gomez MF, Bosc LV, Stevenson AS, Wilkerson MK, Hill-Eubanks DC, Nelson MT: Constitutively elevated nuclear export activity opposes Ca2+-dependent NFATc3 nuclear accumulation in vascular smooth muscle: role of JNK2 and Crm-1. The Journal of biological chemistry 2003;278:46847-46853
41. Awla D, Zetterqvist AV, Abdulla A, Camello C, Berglund LM, Spegel P, Pozo MJ, Camello PJ, Regner S, Gomez MF, Thorlacius H: NFATc3 regulates trypsinogen activation, neutrophil recruitment, and tissue damage in acute pancreatitis in mice. Gastroenterology 2012;143:1352-1360 e1351-1357
42. Yuan Q, Yang J, Santulli G, Reiken SR, Wronska A, Kim MM, Osborne BW, Lacampagne A, Yin Y, Marks AR: Maintenance of normal blood pressure is dependent on IP3R1-mediated regulation of eNOS. Proceedings of the National Academy of Sciences of the United States of America 2016;113:8532-8537
43. Li H, Rao A, Hogan PG: Interaction of calcineurin with substrates and targeting proteins. Trends in cell biology 2011;21:91-103
44. Johnson RS, Titze J, Weller R: Cutaneous control of blood pressure. Current opinion in nephrology and hypertension 2016;25:11-15
45. Nieves-Cintron M, Amberg GC, Nichols CB, Molkentin JD, Santana LF: Activation of NFATc3 down-regulates the beta1 subunit of large conductance, calcium-activated K+ channels in arterial smooth muscle and contributes to hypertension. The Journal of biological chemistry 2007;282:3231-3240
46. Amberg GC, Rossow CF, Navedo MF, Santana LF: NFATc3 regulates Kv2.1 expression in arterial smooth muscle. J Biol Chem 2004;279:47326-47334
47. Mowbray M, McLintock S, Weerakoon R, Lomatschinsky N, Jones S, Rossi AG, Weller RB: Enzyme-Independent NO Stores in Human Skin: Quantification and Influence of UV Radiation. Journal of Investigative Dermatology 2009;129:834-842

Figure Legends

Figure 1. *In vivo* treatment with the NFAT blocker A-285222 restores endothelial function in diabetic mice. (A) Study protocol: Akita mice were randomized based on body weight to receive daily i.p. injections of A-285222 (0.29 mg/kg) or vehicle (saline) for 4 weeks (hatched bar) and skin microvascular responses were assessed blinded either before (Pre), directly after (Post-1) or 4 weeks after the end of treatment (Post-2). **(B)** Blood flow changes in response to iontophoresis of 1% phenylephrine (PE) for 5 min (current 100 μA) followed by iontophoresis of 2% ACh for 10 min (current 100 μA) in Akita vs. WT mice, ***p<0.001. **(C-E)** Microvascular responses to PE and ACh iontophoresis in mice treated as in A, before treatment (n.s., **C**), directly after treatment (*p<0.05, **D**) and 4 weeks after (**p<0.01, **E**). Data in B-E are presented as % of baseline blood flow, as determined prior to initiation of iontophoresis. **(F)** Maximum responses to ACh at each time-point, calculated as the difference between maximum vasodilation to ACh and maximum vasoconstriction to PE (**p<0.01 Akita A-285222 vs. vehicle). **(G)** Blood glucose and **(H)** body weight during the study protocol. N=8-22 mice/group.

Figure 2. Improved skin microvascular function by A-285222 is NO dependent. (A) Summarized data showing skin microvascular response to iontophoresis of ACh after pre-treatment with L-NAME (i.p.; 20 mg/kg body weight), 30 min prior to laser Doppler imaging. Dashed line represents the ACh response in A-285222 treated mice in the absence of L-NAME at the same time point. **(B)** Summarized data showing skin microvascular response to iontophoresis of 2% SNP iontophoresed for 10 min (current=100 μA). Dashed line represents the ACh response in vehicle-treated mice in the absence of SNP at the same time point. Data in A-B are the difference between maximum vasodilation to ACh or SNP and maximum

vasoconstriction to phenylephrine (PE). **(C-D)** Skin microvascular response to localized heating (42°C; 1°C/min) in Akita mice before (n.s., **C**) and immediately after treatment (*p<0.05, **D**) as described in Figure 1A. Data is presented as % of basal blood flow prior to heating. **(E)** Summarized data from measurements in (**D**) showing the maximum vasodilation in response to localized heating, ***p<0.001 **(F)** Longitudinal change in maximum vasodilation in response to localized heating expressed as the difference between measurements before (Pre) and after (Post-1) treatment with A-285222 or vehicle, ***p<0.001. N=5-16 mice/group.

Figure 3. **NFATc3 is the predominant NFAT isoform expressed in mouse skin. (A)** Whole mouse skin flat preparation (dermis face up) showing skin microvessels and a dashed circle representing the size of the area analyzed in laser Doppler imaging experiments. Scale bar=5 mm. **(B)** H&E stained cross sections of mouse skin showing microvessels (arrowheads) in the dermis layer ("D"). Epidermis ("E"); scale bars upper panels=500 μm, lower panels=100 μm. **(C)** Absolute quantification of NFATc1-c4 mRNA in dermis and epidermis from non-diabetic C57Bl/6J mice, expressed as billion (10^9) copies per μg total RNA. N=3 mice/preparation. **(D)** Gene expression analysis of NFATc1-c4 isoforms mRNA by qPCR in the dermis from non-diabetic WT/NFAT-luc and diabetic Akita/NFAT-luc mice. N=5 mice/group **(E)** Representative confocal images of skin whole mounts showing CD31 and NFATc3 (red) staining in microvessels. Nuclei are stained with SYTOX Green. Bar=50 μm. **(F)** NFAT-dependent transcriptional activity in dermis ("D") and epidermis ("E") homogenates from NFAT-luc mice, expressed as relative luciferase units (RLU) per μg of protein. Dashed line indicates NFAT-dependent transcriptional activity in whole skin. N=5 mice/group. **(G)** Representative immunoblot showing expression of CD31 in whole skin

("WS"), dermis ("D") and epidermis ("E") from non-diabetic C57Bl/6J mice. α-tubulin was used as loading control.

Figure 4. A-285222 decreases NFATc3 nuclear accumulation in skin microvessels. **(A)** Representative confocal images showing NFATc3 nuclear accumulation in skin microvessels from Akita mice 4 weeks after treatment with vehicle (upper panels) and A-285222 (lower panels) as described in Figure 1A. Left panels in both rows are pseudo colored images showing NFATc3 nuclear accumulation in white; middle and right panels are original images showing the DNA binding dye SYTOX Green (green) and NFATc3 (red), respectively. Scale bar=10 μm. **(B)** Summarized data from experiments in A showing percentage of cells exhibiting NFATc3 nuclear accumulation in skin microvessels (*$p<0.05$). N=5-7 mice/group with at least 100 cells examined per animal. **(C)** NFAT-dependent transcriptional activity in whole skin homogenates from wild type (WT)/NFAT-luc and Akita/NFAT-luc mice 9 weeks after completion of the treatment with A-285222 (0.29 mg/kg and day for 4 weeks) or vehicle. Data is expressed as relative luciferase units (RLU) per μg of protein. **(D)** Gene expression analysis of luciferase mRNA by qPCR in dermis from WT/NFAT-luc and Akita/NFAT-luc mice after treatment as in (C). HPRT and cyclophilin B were used as endogenous controls and data is expressed as percentage of vehicle treated WT/NFAT-luc mice. *$p<0.05$ vs WT and $^{\#}p<0.05$ vs Akita. N=4-7 mice/group.

Figure 5. NFAT inhibition with A-285222 enhances eNOS expression and plasma NO levels. (A) Gene expression analysis of eNOS mRNA by qPCR in dermis from WT/NFAT-luc and Akita/NFAT-luc mice directly after (Post-1) and 9 weeks after (Post-2) treatment with A-285222 or vehicle. HPRT and cyclophilin B were used as endogenous controls and data is expressed as percentage of vehicle treated WT/NFAT-luc mice. N=4-10 mice/group **(B)**

Summarized data and representative immunoblots from Western blot experiments showing eNOS (left) and p-eNOS (middle) protein expression, as well as p-eNOS/eNOS ratio (right) in the dermis of non-diabetic WT/NFAT-luc and diabetic Akita/NFAT-luc mice, 9 weeks after A-285222 or vehicle treatment. Results are expressed as percentage of vehicle treated WT/NFAT-luc mice. *p<0.05 and **p<0.01 vs WT. N=11-15 mice/group. **(C)** Plasma nitric oxide (NO) levels in Akita mice four weeks after treatment with A-285222 or vehicle as described in Figure 1A. N=5 mice/group **(D)** Immunohistochemistry images showing eNOS protein expression in skin microvessels directly after treatment with A-285222 (Post-1) as described in A. Bar=5 μm. **(E-F)** Gene expression analysis of luciferase (D) and eNOS (E) mRNA in dermis from WT/NFAT-luc mice after 24h whole skin organ culture in the presence or absence of A-285222 (1 μmol/L. *p<0.05 and **p<0.01 vs vehicle treated mice of the same genotype). N=7-8 mice/group. **(G)** Summarized data from Western blot experiments showing eNOS (left) and p-eNOS (middle) protein expression, as well as p-eNOS/eNOS ratio (right) in the dermis after whole skin organ culture for 48h with or without A-285222 (1 μmol/L). Included also is a representative immunoblots of eNOS and p-eNOS protein expression in fresh and cultured dermis with or without A-258222. Data is expressed as percentage of the fresh sample. *p<0.05; N=10 for fresh and N=8 mice/group for cultured samples.

Figure 6. NFAT inhibition with A-285222 prevents diabetes-induced increase of inflammatory plasma cytokines and endothelial activation markers. Summarized plasma levels of **(A)** IL-6, **(B)** osteopontin, **(C)** sICAM, **(D)** IL-1α, **(E)** IL-10 and **(F)** E-selectin in Akita mice measured before (Pre), directly after (P1= Post-1), and four weeks after (P2= Post-2) treatment with A-285222 (0.29 mg/kg and day) or vehicle as outlined in Figure 1A. *p<0.05, **p<0.01 and ***p<0.001 vs Akita. N=6-22 mice/group.

Figure 7. *In vivo* treatment with A-285222 improves blood pressure and survival in Akita mice. **(A)** Plasma endothelin-1 levels four weeks after (Post-2) treatment with A-285222 (0.29 mg/kg and day) or vehicle as outlined in Figure 1A. N=13-15 mice/group. **(B)** Systolic and **(C)** diastolic blood pressure measured non-invasively four weeks after A-285222 treatment as described in (A); *p<0.05 and **p<0.01. N=4-7 mice/group. **(D)** Kaplan-Meier curves showing survival of Akita mice treated with A-285222 or vehicle as described in Figure 1A (p=0.0817). N=7-8 mice/group **(E)** Kaplan-Meier curve showing survival data from an independent study conducted for another project (C57BL/6J background; mixed genders) treated as outlined in Figure 1A (p=0.0299). Mean age at the start of the experiments=14 weeks; N=15-18 mice/group.

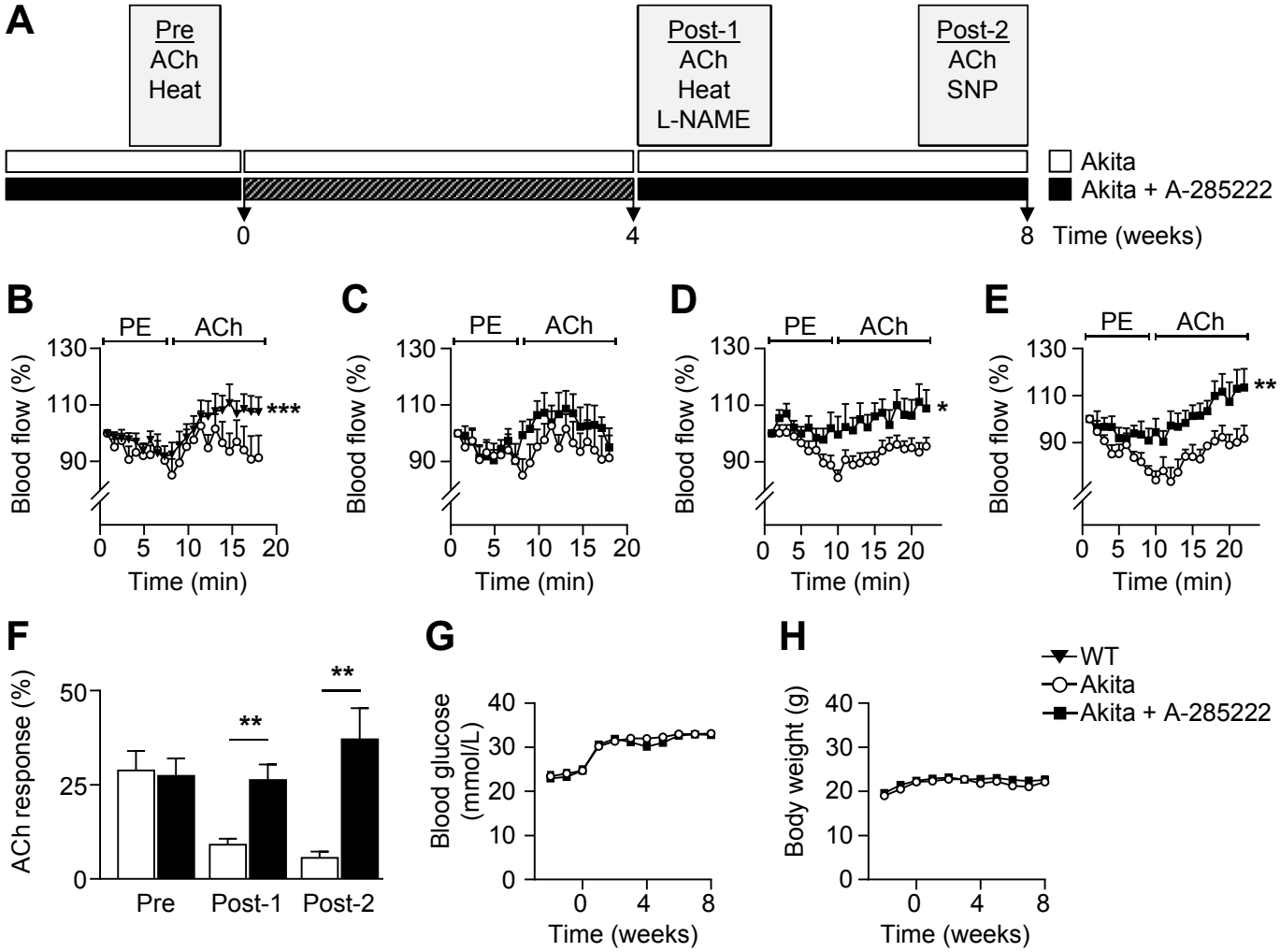
A
Pre
ACh
Heat
Post-1
ACh
Heat
L-NAME
Post-2
ACh
SNP
Akita
Akita + A-285222
0
4
8
Time (weeks)
B
C
D
E
PE
ACh
Blood flow (%)
130
110
90
0 5 10 15 20
Time (min)
***
*
**
F
ACh response (%)
50
25
0
Pre
Post-1
Post-2
G
Blood glucose (mmol/L)
40
30
20
10
0
0 4 8
Time (weeks)
H
Body weight (g)
WT
Akita
Akita + A-285222

Figure 1

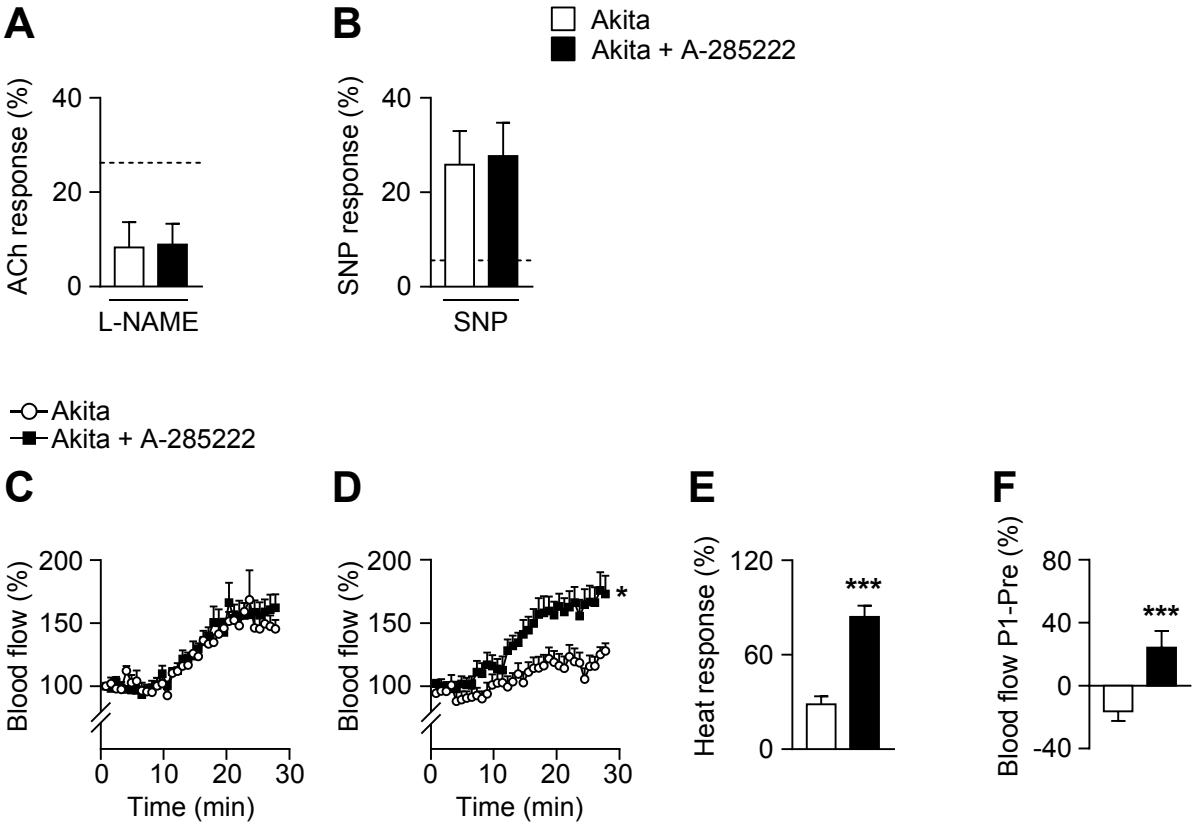
A
B
Akita
Akita + A-285222
ACh response (%)
40
20
0
L-NAME
SNP response (%)
SNP
Akita
Akita + A-285222
C
D
E
F
Blood flow (%)
200
150
100
0
10
20
30
Time (min)
*
Heat response (%)
120
60
***
Blood flow P1-Pre (%)
80
40
-40

Figure 2

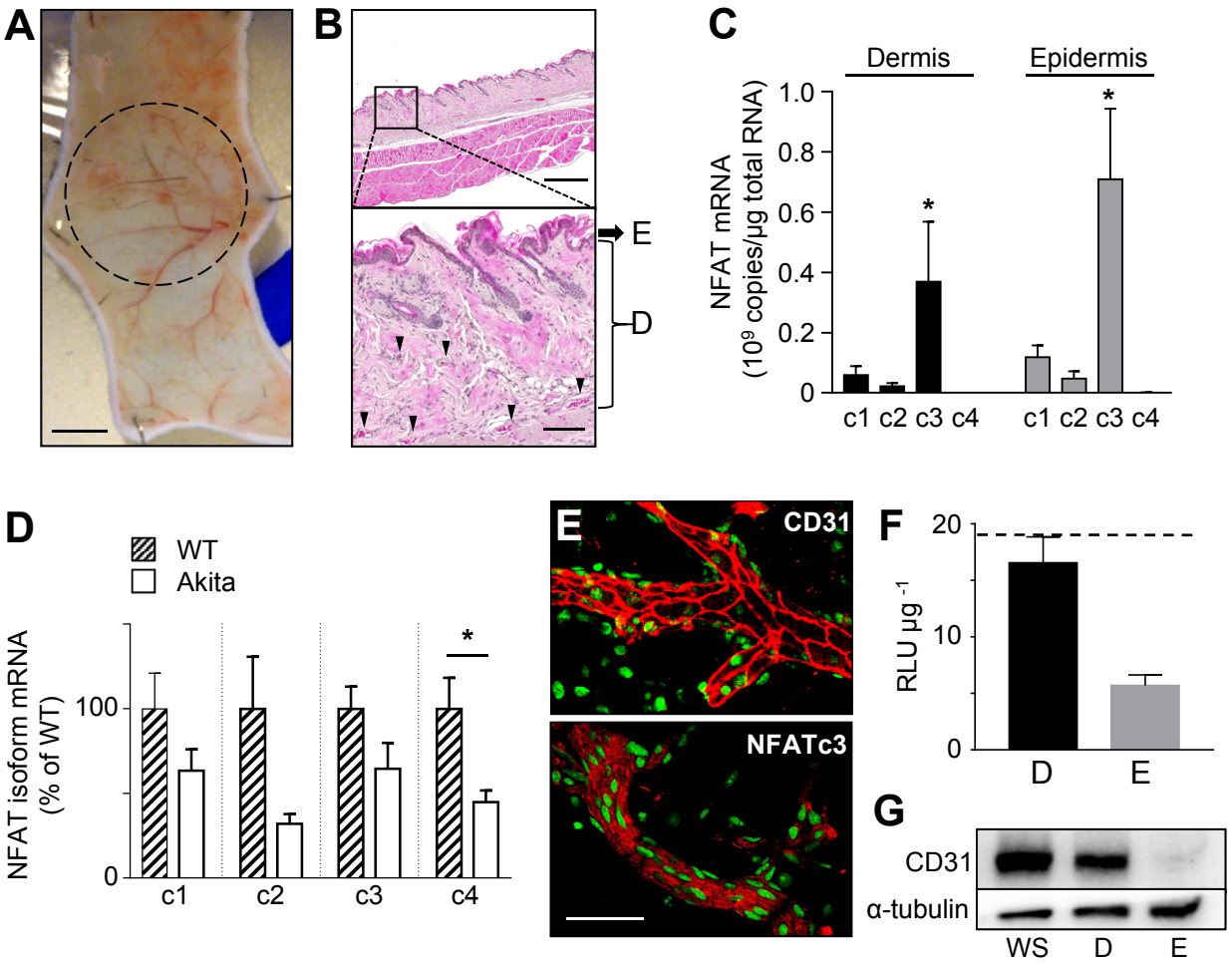
A
B
E
D
C
Dermis
Epidermis
NFAT mRNA
(10⁹ copies/µg total RNA)
1.0
0.8
0.6
0.4
0.2
0
*
*
c1 c2 c3 c4
c1 c2 c3 c4
D
WT
Akita
NFAT isoform mRNA
(% of WT)
100
0
*
c1
c2
c3
c4
E
CD31
NFATc3
F
RLU µg⁻¹
20
10
0
D
E
G
CD31
α-tubulin
WS
D
E

Figure 3

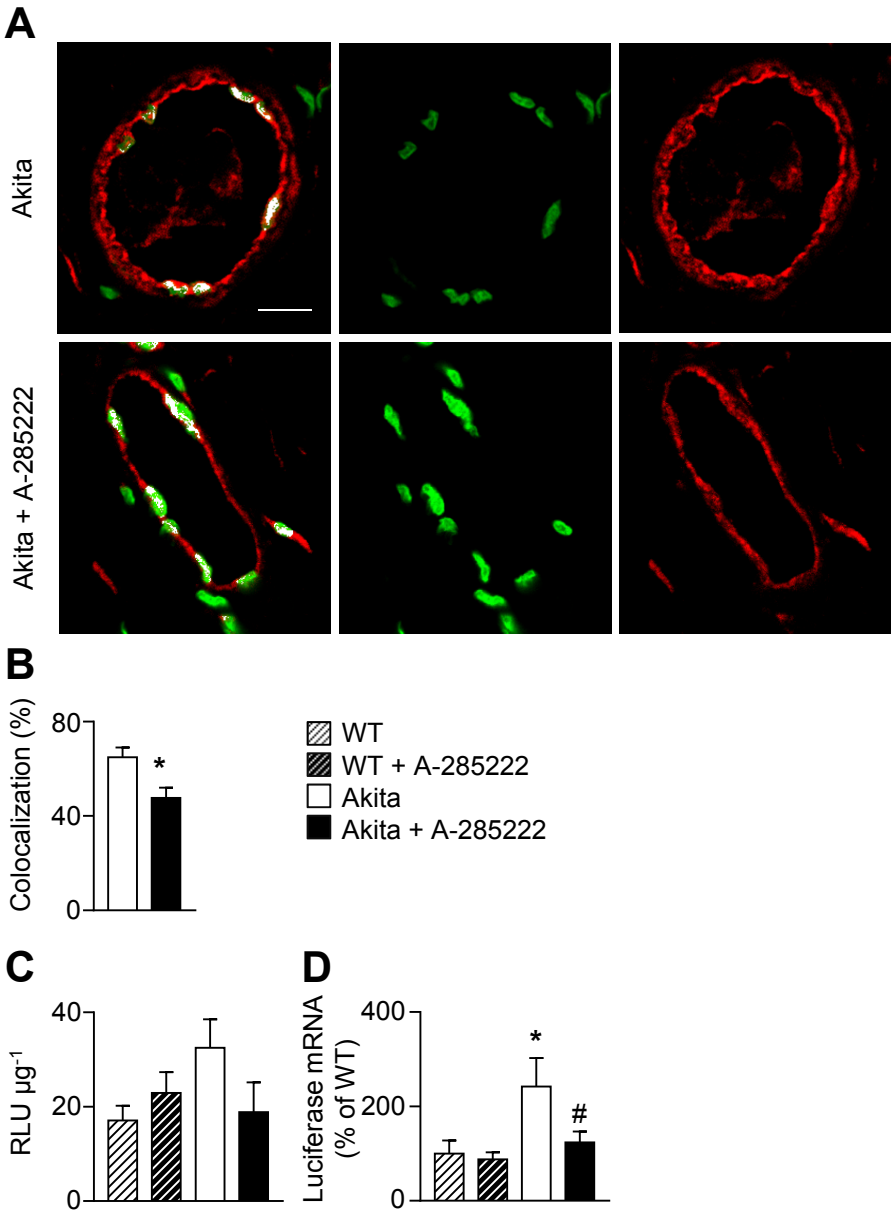
A
Akita
Akita + A-285222
B
Colocalization (%)
80
40
0
*
WT
WT + A-285222
Akita
Akita + A-285222
C
RLU µg-1
40
20
0
D
Luciferase mRNA (% of WT)
400
200
0
*
#

Figure 4

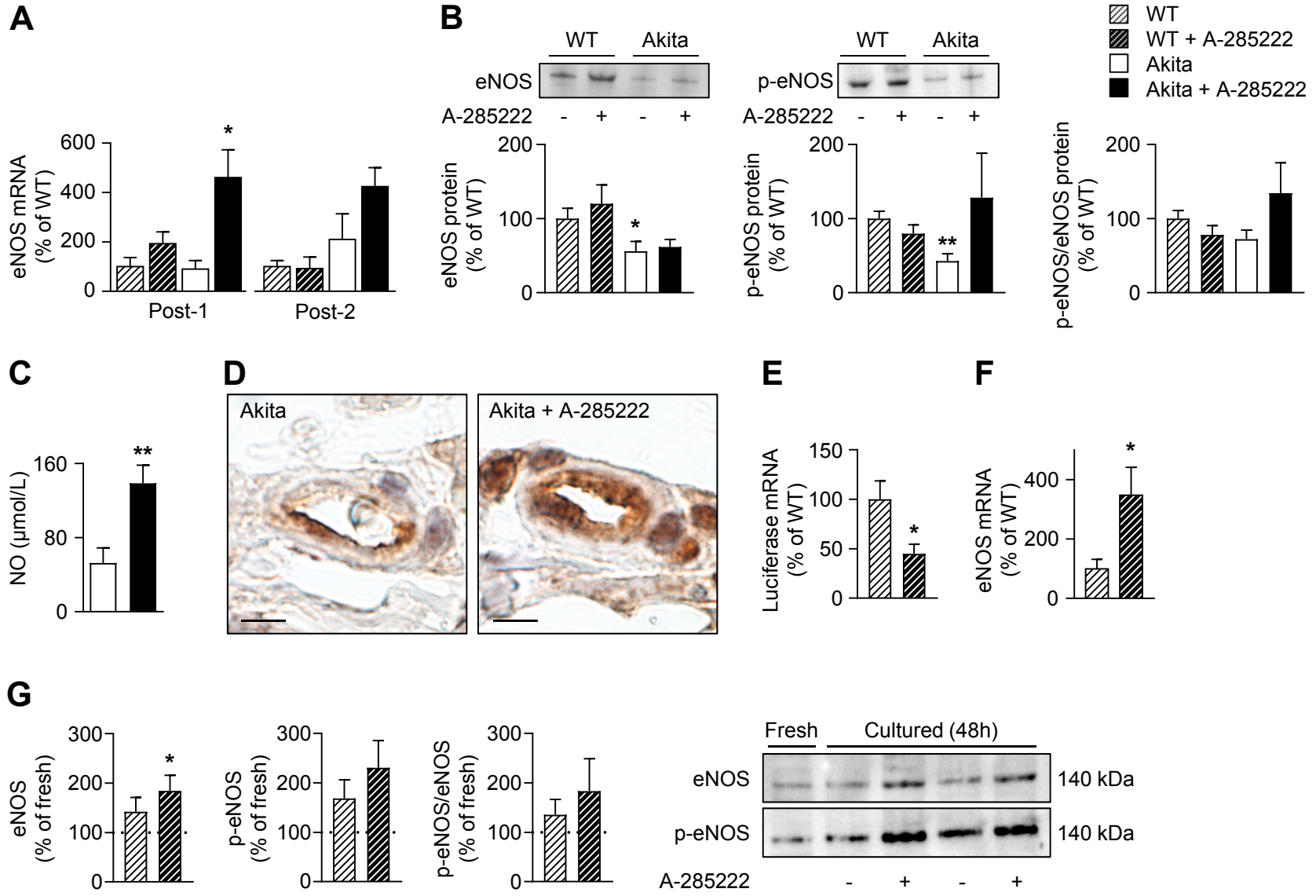
A
eNOS mRNA (% of WT)
600
400
200
0
*
Post-1
Post-2
B
WT
Akita
eNOS
A-285222 - + - +
eNOS protein (% of WT)
200
100
0
*
p-eNOS
p-eNOS protein (% of WT)
**
p-eNOS/eNOS protein (% of WT)
WT
WT + A-285222
Akita
Akita + A-285222
C
NO (µmol/L)
160
80
0
**
D
Akita
Akita + A-285222
E
Luciferase mRNA (% of WT)
150
100
50
0
*
F
eNOS mRNA (% of WT)
400
200
0
*
G
eNOS (% of fresh)
p-eNOS (% of fresh)
p-eNOS/eNOS (% of fresh)
300
200
100
0
*
Fresh
Cultured (48h)
eNOS
p-eNOS
140 kDa
140 kDa
A-285222 - + - +

Figure 5

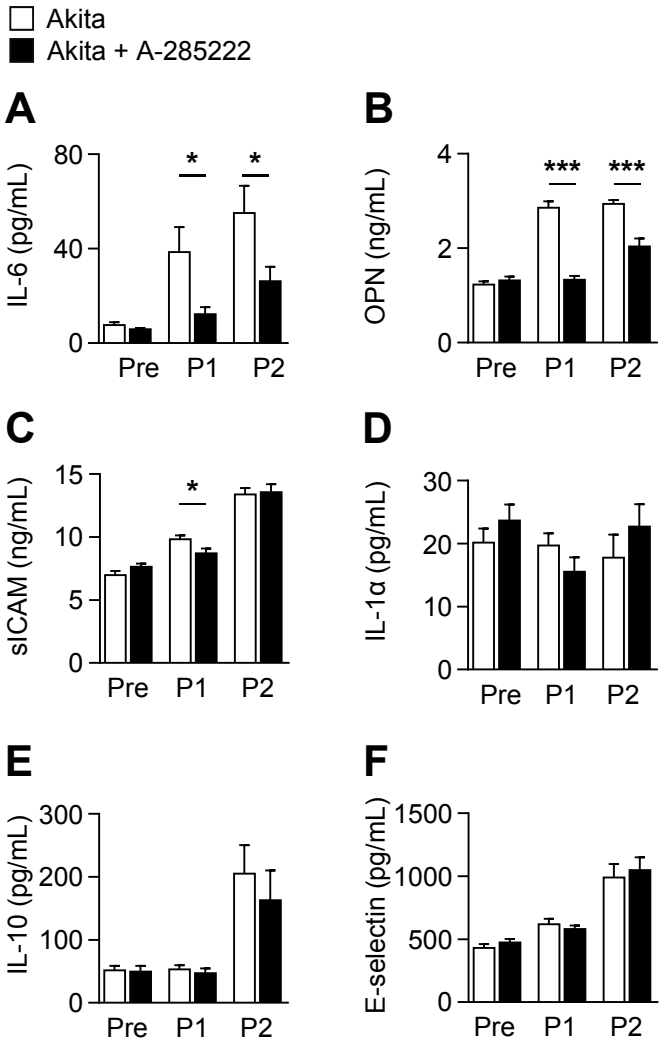
Akita
Akita + A-285222
A
IL-6 (pg/mL)
80
40
0
*
*
Pre
P1
P2
B
OPN (ng/mL)
4
2
0
***
***
Pre
P1
P2
C
sICAM (ng/mL)
15
10
5
0
*
Pre
P1
P2
D
IL-1α (pg/mL)
30
20
10
0
Pre
P1
P2
E
IL-10 (pg/mL)
300
200
100
0
Pre
P1
P2
F
E-selectin (pg/mL)
1500
1000
500
0
Pre
P1
P2

Figure 6

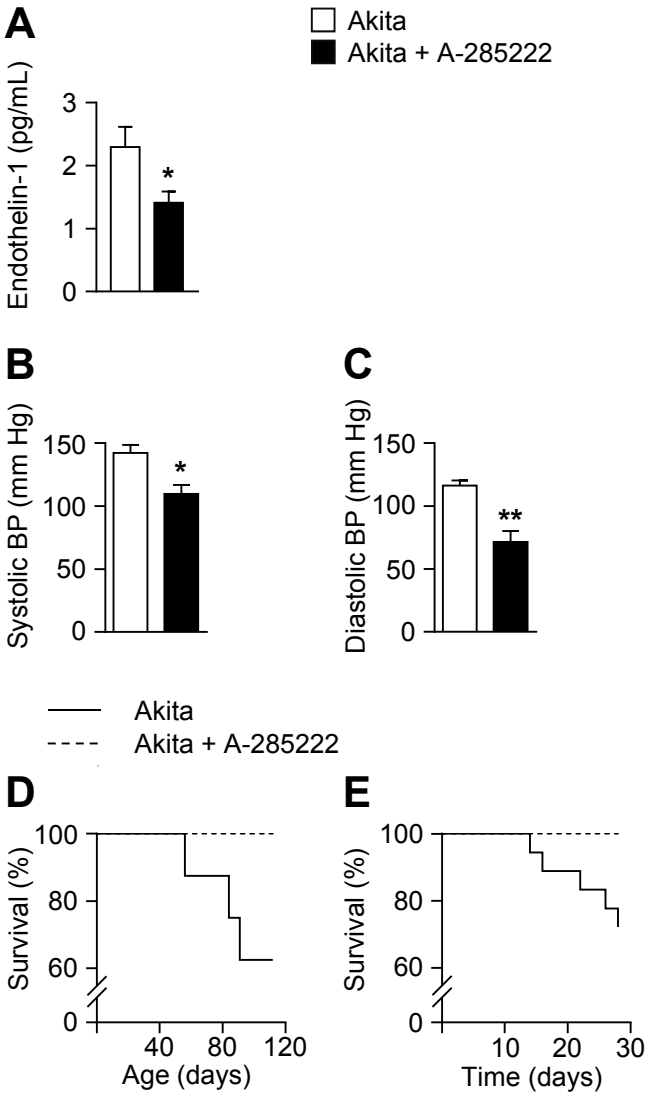
A
Akita
Akita + A-285222
Endothelin-1 (pg/mL)
3
2
1
0
*
B
Systolic BP (mm Hg)
150
100
50
0
*
C
Diastolic BP (mm Hg)
150
100
50
0
**
Akita
Akita + A-285222
D
Survival (%)
100
80
60
0
40
80
120
Age (days)
E
Survival (%)
100
80
60
0
10
20
30
Time (days)

Figure 7

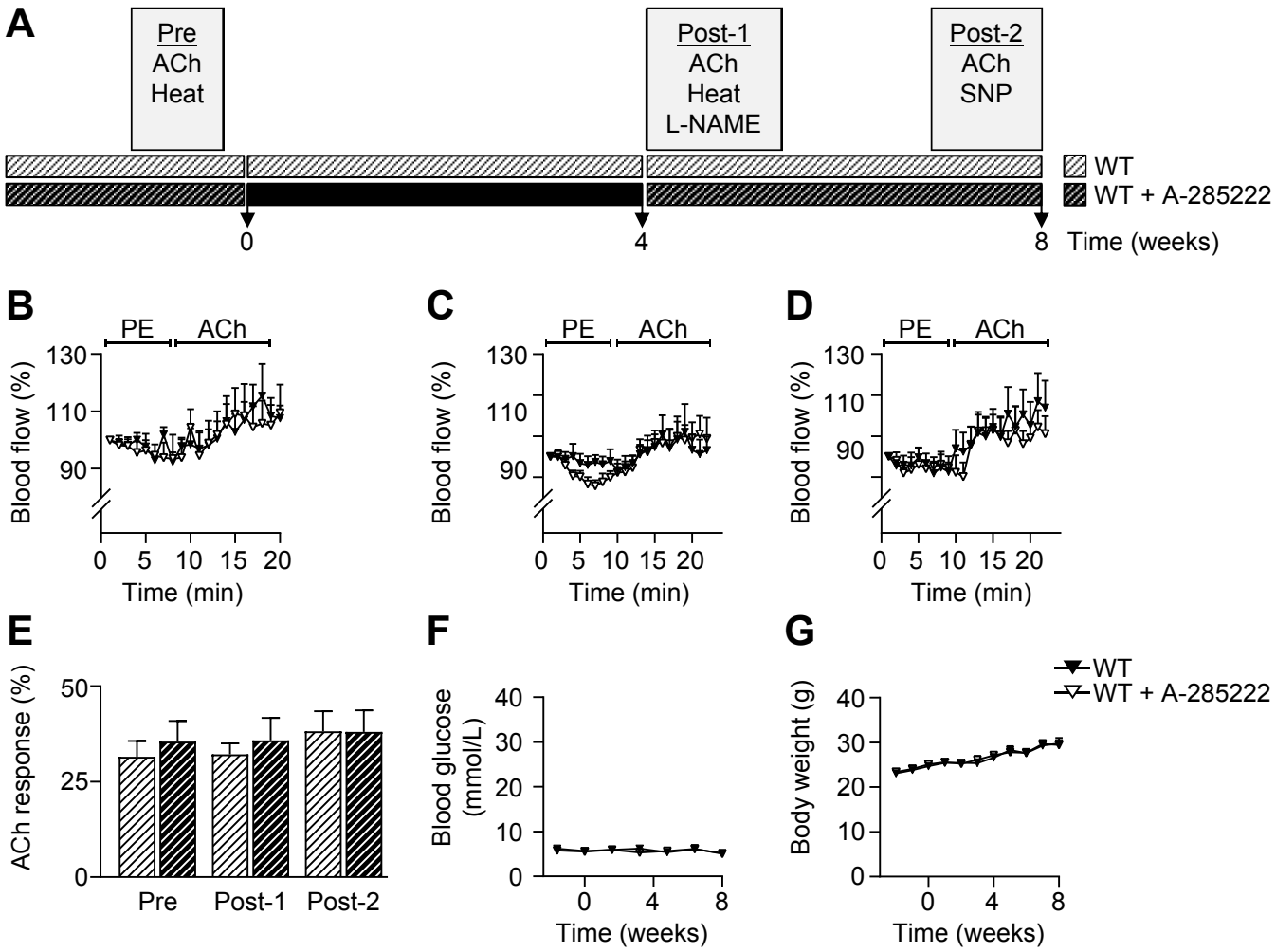

Figure S1. ***In vivo*** **treatment with the NFAT blocker A-285222 has no effect on skin microvascular responses to acetylcholine, blood glucose levels or body weight in non-diabetic wild-type mice (A)** Study protocol: Wild type mice received daily i.p. injections of A-285222 (0.29 mg/kg) or vehicle (saline) for 4 weeks (black bar) and skin microvascular responses were assessed either before (Pre), directly after (Post-1) or 4 weeks after the end of treatment (Post-2). **(B-D)** Microvascular responses to iontophoresis of phenylephrine (PE) and acethylcholine (ACh) in mice treated as in A, before treatment (**B**), directly after treatment (**C**) and 4 weeks after (**D**). Data in B-D are presented as % of baseline blood flow, as determined prior to initiation of iontophoresis. **(E)** Maximun responses to ACh at each time-point, calculated as the difference between maximum vasodilation to ACh and maximum vasoconstriction to PE. **(F)** Blood glucose and **(G)** body weight during the study. N=7-10 mice/group.

Figure S1

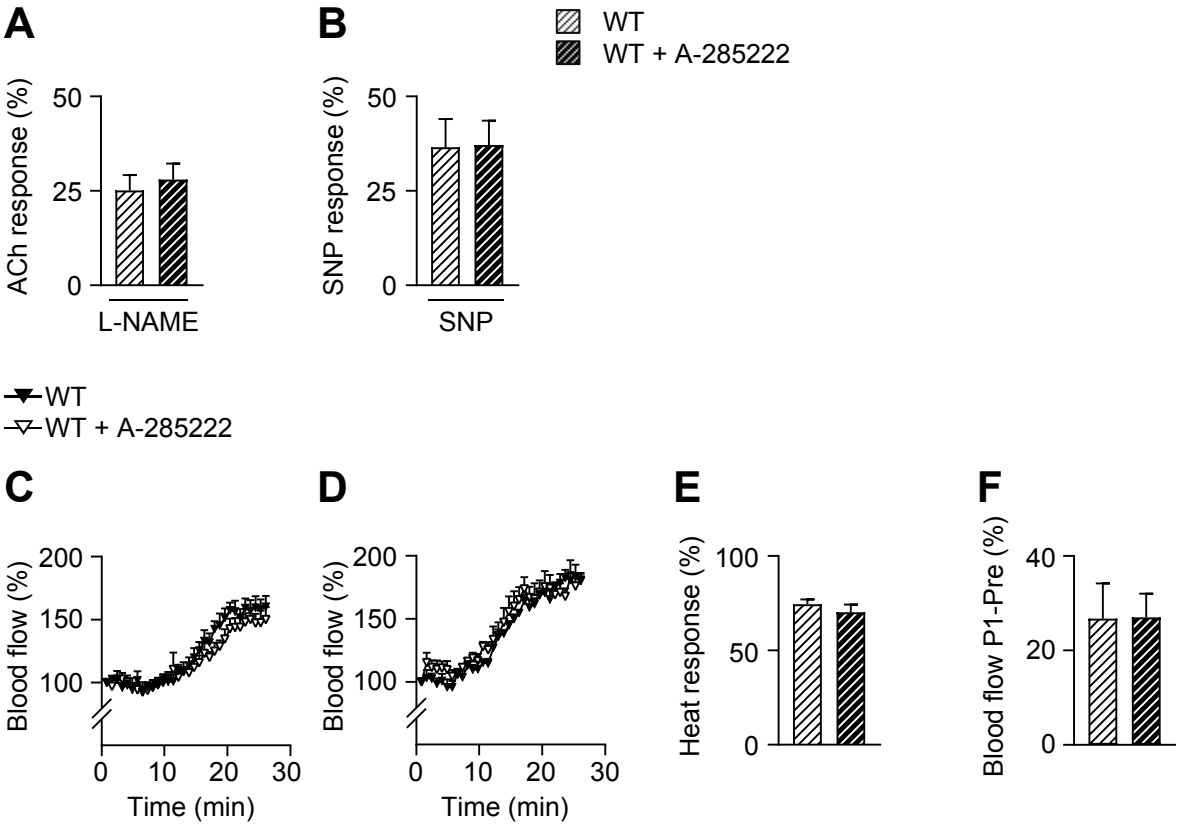

Figure S2. **Treatment with the NFAT blocker A-285222 has no effect on skin microvascular responses to localized heating in non-diabetic wild-type (WT) mice**. **(A)** Skin microvascular response to iontophoresis of ACh after pre-treatment with L-NAME (i.p. 20 mg/kg body weight) were not affected after A-285222 treatment in WT mice. **(B)** Summarized data showing skin microvascular response to iontophoresis of SNP. Data showed in A and B are the difference between maximum vasodilation to ACh or SNP and maximum vasoconstriction to phenylephrine (PE). Microvascular response to localized heating (42^{o}C, 1^{o}C/min) in WT mice before **(C)** and immediately after treatment (**D**). Data is presented as % of basal blood flow prior to heating. **(E)** Summarized data from measurements in (D) showing the maximum vasodilation in response to localized heating. **(F)** Longitudinal change in maximum vasodilation in response to localized heating expressed as the difference between measurements before (Pre) and after (Post-1) treatment with A-285222 or vehicle, N=6-9 mice/group.

Figure S2

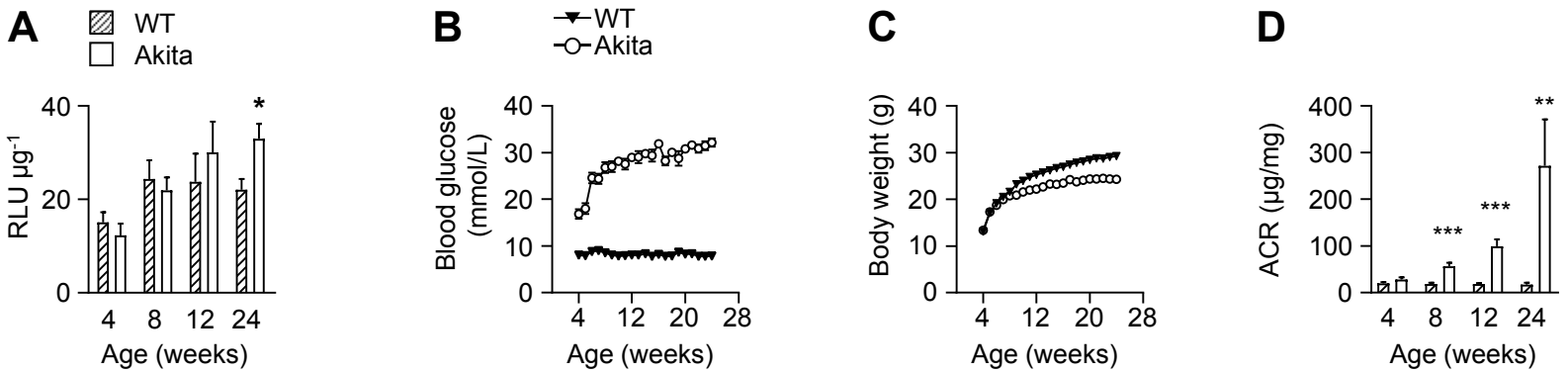

Figure S3. **Age-dependent increase in NFAT transcriptional activity in the skin of Akita mice. (A)** Diabetic Akita/NFAT-luc and non-diabetic WT/NFAT-luc littermate mice were euthanized at 4, 8, 12 and 24 weeks of age (N=6 mice/group) and skin harvested for measurements of NFAT-dependent transcriptional activity. Data is expressed as relative luciferase units (RLU) per µg of protein. **(B-D)** Animals in (A), along with non-TG littermates were monitored weekly for blood glucose (B), body weight (C) and urine was collected for measurements of albumin-to-creatinine ratio (ACR, D). *p<0.05, **p<0.01 and ***p<0.001 vs. WT. N=6-13 mice/group.

Figure S3

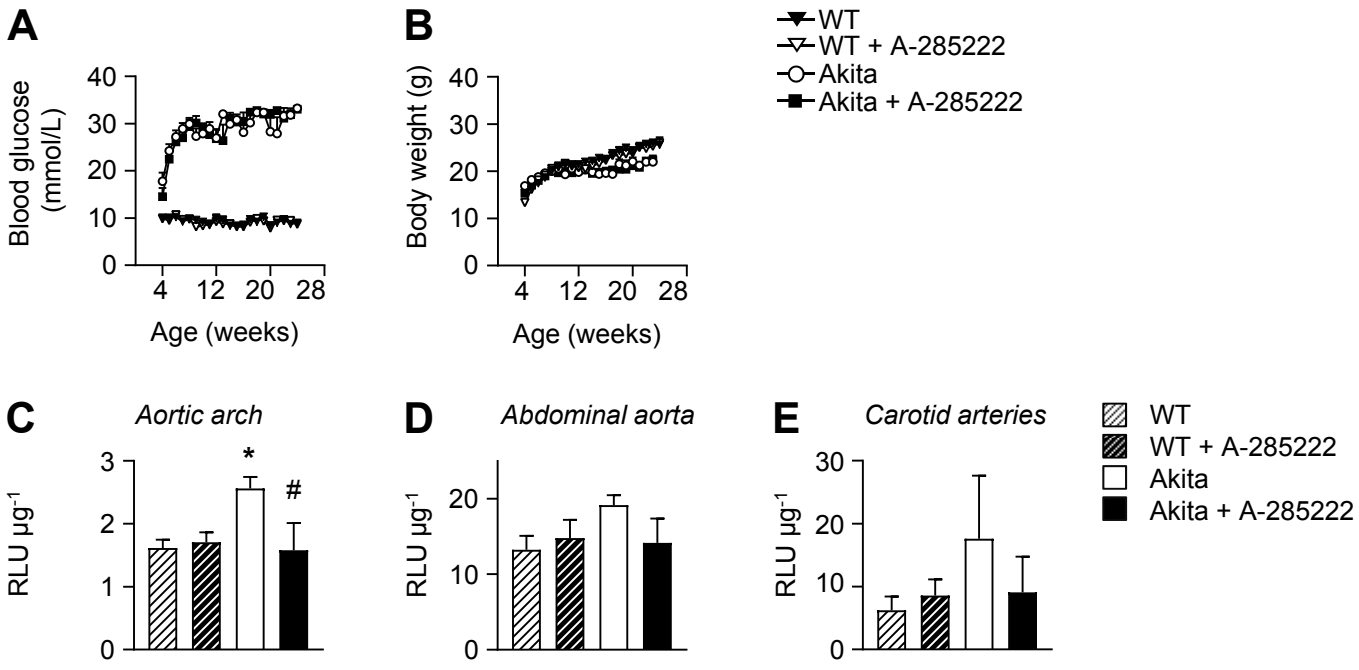

Figure S4. **NFAT-dependent transcriptional activity is increased in vessels from diabetic Akita mice and this is prevented by treatment with A-285222**. **(A)** Blood glucose and **(B)** body weight monitored weekly in WT/NFAT-luc and Akita/NFAT-luc mice treated with vehicle or A-285222 (0.29 mg/kg and day during weeks 11-15 of age). N=4-16 mice/time-point. **(C-E)** NFAT luciferase activity was measured in the aortic arch (C), abdominal aorta (D), and carotid arteries (E) from mice described in A-B. Data is expressed as relative luciferase units (RLU) per µg of protein. *p<0.05 vs. WT and #p<0.05 vs. Akita. N=4-7 mice/group.

Figure S4

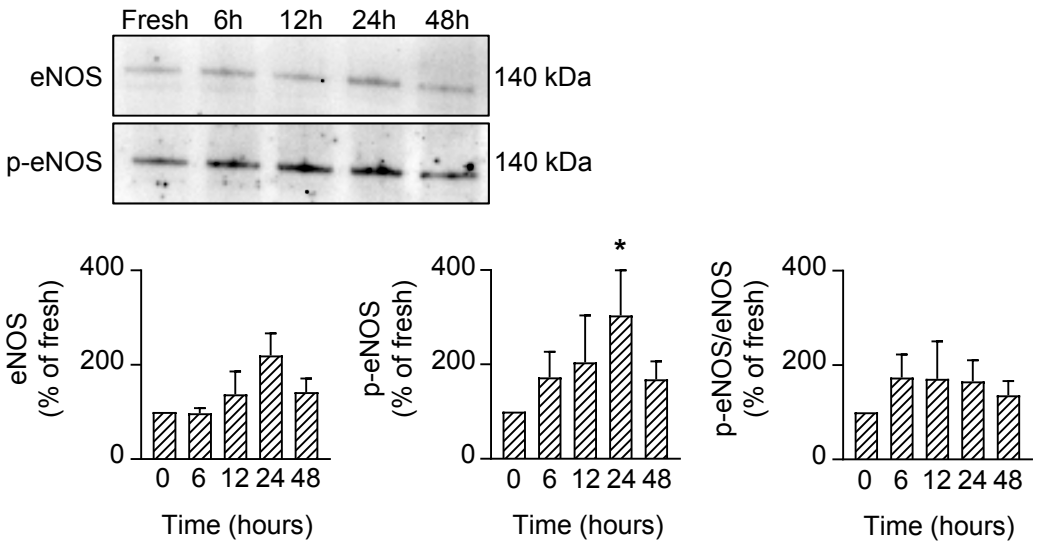

Figure S5. **Time-dependent effects on eNOS and p-eNOS protein expression in the dermis during organ culture of skin intact samples.** Intact skin samples from non-diabetic mice were frozen either fresh or after culture for 6, 12, 24 and 48 hours in DMEM**.** Upper panels show representative immunoblots for eNOS and p-eNOS protein for fresh tissue and for the various time points in culture. Graphs below show summarized results from western blot experiments for eNOS and p-eNOS normalized to total protein and for p-eNOS/eNOS ratio. Data is expressed as percentage of the fresh sample for each animal to assess whether culture per se and/or time in culture had any impact on expression, irrespective of the basal level of expression in each animal before culture. Expression of p-eNOS was significantly increased at 24h (*$p<0.05$; N=10 for fresh, N=4 mice/group for 6 and 12h and N=8 mice/group for 24 and 48h).

Figure S5

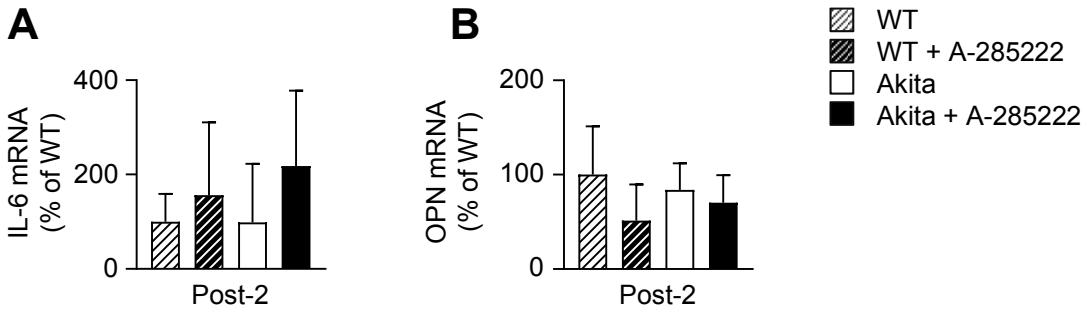

Figure S6 No significant changes in the expression of OPN or IL-6 in the dermis of diabetic Akita and non-diabetic wild-type mice after *in vivo* treatment with A-285222. Gene expression analysis of IL-6 **(A)** and osteopontin **(B)** mRNA by qPCR in dermis from WT/NFAT-luc and Akita/NFAT-luc mice after treatment ("Post-2") with A-285222 NFAT blocker or vehicle. HPRT and cyclophilin B were used as endogenous controls and data is expressed as percentage of vehicle treated WT/NFAT-luc mice. N=4-7 mice/group.

Figure S6

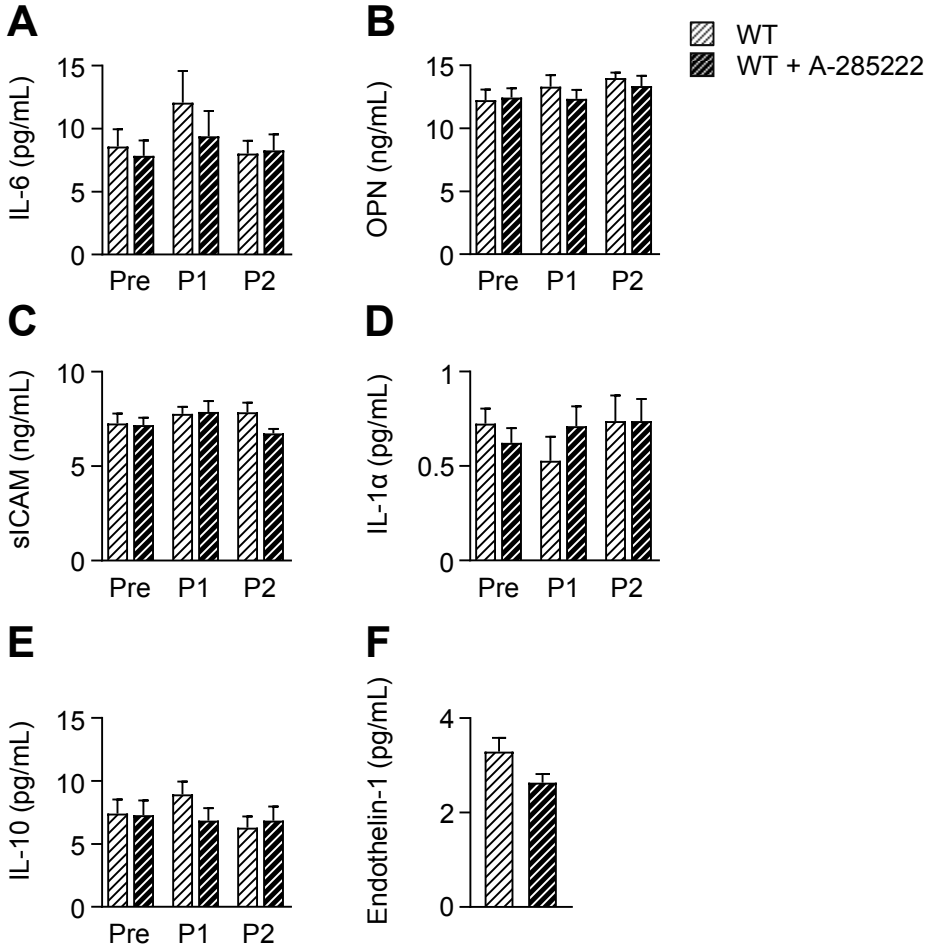

Figure S7. **NFAT inhibition with A-285222 has no effect on the levels of circulating plasma cytokines in non-diabetic wild-type (WT) mice**. **(A)** Plasma levels of **(A)** IL-6, **(B)** osteopontin, **(C)** sICAM, **(D)** IL-1α, **(E)** IL-10 and **(F)** Endothelin-1 in WT mice measured before (Pre), directly after (P1=Post-1), and four weeks after (P2= Post-2) treatment with A-285222 (0.29 mg/kg a day) or vehicle. N=6-9 mice/group.

Figure S7

Online Data Supplement

Adult heterozygous diabetic Akita (*Ins2*$^{+/-}$) mice were used (stock number 007562; D2.B6 background; The Jackson Laboratory, Maine). FVBN 9x-Nuclear Factor of Activated T-cells (NFAT)-luciferase reporter (NFAT-luc) mice[1-3] and Akita mice (stock number 003548, C57BL/6J background, The Jackson Laboratory) were used to generate Akita/NFAT-luc mice and non-diabetic wild-type (WT)/NFAT-luc littermates, backcrossed at least four generations into the C57BL/6J background. Animals had free access to tap water and were fed normal chow diet. Blood glucose (CONTOUR® meter; Bayer) and body weight were monitored weekly. Because of the limited hyperglycemia observed in Akita female mice, male mice were studied for all parts of the study except for the Kaplan-Meier survival curves in Figure 7E that includes data from both sexes. Mice were euthanized by cervical dislocation after anesthesia with 3% isoflurane in oxygen (2 L/min). For NFAT-luciferase experiments, mice were anaesthetized by intraperitoneal (i.p.) injection of 7.5 mg ketamine hydrochloride and 2.5 mg xylazine per 100 g body weight and euthanized by exsanguination through cardiac puncture. All animal protocols in this study were performed in accordance with UK Home Office regulations (Project License PIL60/4265) and the Malmö/Lund Animal Care and Use Committee (Permits M78-10, M29-12, and M9-15) and abided by the Guide for the Care and Use of Laboratory Animals published by the Directive 2010/63/EU of the European Parliament.

Laser Doppler imaging, iontophoresis and localized heating

The study protocol is shown in **Figure 1A**. Akita mice were randomized based on body weight to receive daily i.p. injections of the NFAT blocker A-285222 (0.29 mg/kg body weight) or vehicle (saline) for 4 weeks. Microvascular function was assessed blinded and non-invasively, before ("Pre"; at 7-12 weeks of age), directly after ("Post-1")- or 4 weeks after ("Post-2") the end of the treatment, using a laser Doppler imager (LDI; moorLDI, Moor Instruments Ltd, Axminster, UK) as previously described [4, 5]. In brief, 2 days prior to the measurements, fur was removed from the flank area of the mouse by shaving and with depilatory cream (Veet® Reckitt-Benckiser, Søborg, Danmark). General anesthesia was induced (5% isoflurane in 2 L/min oxygen) and maintained during the procedures (1.5-2% isoflurane in 1.5 L/min oxygen), and body temperature was maintained at 37°C using a heat mat.

For assessing microvascular responses to acetylcholine (ACh), an iontophoresis chamber (ION6 probe, Moor Instruments Ltd, Axminster, UK) was attached to the flank and a reference electrode pad attached to the underside of the animal to complete the iontophoresis circuit. To standardize basal perfusion, blood vessels were pre-constricted with iontophoresis of 1% phenylephrine (PE) for 5 min (current=100 μA), followed by iontophoresis of 2% ACh for 10 min (current=100 μA). At a different site on the opposite flank, 2% sodium nitroprusside (SNP) was iontophoresed for 10 min (current=100 μA). To determine the contribution of endothelium-derived nitric oxide (NO) to ACh-mediated vasodilatation, microvascular responses to ACh were assessed 30 min after i.p. injection of the non-selective inhibitor of NO synthase, N(G)-nitro-L-arginine methyl ester (L-NAME, Sigma Chemicals; 20 mg/kg). [4] On a separate day and to determine the maximum microvascular dilator capacity, a hyperemic response was initiated by localized heating of the skin using a specially designed heating probe (SH02™ skin heating unit and SHP3 probe, Moor Instruments Ltd, Axminster, UK). Perfusion was measured continuously as the temperature of the heating probe was increased to 42°C (1°C/min) and maintained for >10 min, which was sufficient for maximum vasodilatation to plateau.

The LDI scans continuously during the iontophoresis and localized heating periods and provides a measure of microvascular perfusion (in arbitrary perfusion units). Color-coded images were generated for each perfusion scan and numerical outputs were produced (moorLDI software version 5.2) and analyzed using proprietary software (Moor Instruments, version 5.3). The vascular response to ACh, PE and heating is presented as the percentage change from basal perfusion measured during 5 scans prior to the application of PE or initiation of heating. Endothelium-dependent and –independent vasodilation in response to ACh or SNP, respectively, was calculated as the difference between maximum vasodilation in response to ACh or SNP and maximum vasoconstriction in response to PE.

The response to localized heating was expressed as the percentage change in perfusion from baseline measurements to maximum vasodilation.

NFAT-dependent transcriptional activity

Diabetic Akita/NFAT-luc and non-diabetic WT/NFAT-luc littermate mice were euthanized at 4, 8, 12 and 24 weeks of age (N=6 mice/group) and skin harvested for measurements of NFAT-dependent transcriptional activity. A separate group of Akita/NFAT-luc and WT/NFAT-luc mice received daily i.p. injections of the NFAT blocker A-285222 (0.29 mg/kg body weight) or vehicle (saline) for 4 weeks (starting at 8-11 weeks of age). Mice were euthanized either directly after the treatment or 9 weeks after completion of the treatment. At termination, the aortic arch, abdominal aorta, carotid arteries and skin were collected and dissected free from surrounding tissue in ice-cold Ca^{2+}-free physiological saline solution (PSS; containing in mmol/L: NaCl, 135; KCl, 5.9; MgCl2, 1.2; Hepes, 11.6; glucose, 2.0; pH 7.4). Luciferase activity was measured in tissue homogenates as previously described [2]. Optical density was measured using a Tecan INfinite M200 instrument (Tecan Nordic AB, Mölndal, Sweden) and data is expressed as relative luciferase units (RLU) per µg of protein, as assessed using EZQ protein quantification kit (Molecular Probes, Invitrogen, Paisley, UK) or DC Protein Assay (Bio-Rad Laboratories, Sundbyberg, Sweden).

Histology and confocal microscopy

Skin biopsies from the flank of the mice were fixed overnight in 4% formaldehyde in phosphate-buffered saline (PBS, pH 7.4), and either dehydrated and paraffin embedded for sectioning (5 µm) or processed as whole mounts for immunostaining. Sections were used for histology (hematoxylin and eosin; H&E), for quantification of NFATc3 nuclear accumulation using confocal microscopy or for immunohistochemistry of endothelial nitric oxide synthase (eNOS). For NFATc3 staining, sections were subjected to heat induced epitope retrieval using citrate buffer (10 mmol/L; pH 6.0) and stained as previously described.[1] Briefly, sections were permeabilized with 0.2% Triton X-100 in PBS, blocked for 2h with 2% bovine serum albumin (BSA) in PBS and incubated with rabbit polyclonal anti-NFATc3 (sc-8321, 0.2 µg/mL, Santa Cruz Biotechnology, Santa Cruz, CA) overnight at 4°C, followed by incubation with Cy5 anti-rabbit IgG (3 µg/mL, Jackson Immuno Research, West Grove, PA) for 1h at room temperature. Nuclei were stained with SYTOX green (Molecular Probes, Invitrogen, Paisley, UK). For eNOS staining, sections were incubated with 0.3% H_2O_2 in methanol for 30 min to eliminate endogenous peroxidase activity, then rinsed with PBS, blocked with 10% normal goat serum for 1h and incubated with rabbit polyclonal anti-eNOS antibody (0.125 µg/mL, sc-654 Santa Cruz Biotechnology) or non-immune rabbit IgG (0.125 µg/mL, ab27478, Abcam, Cambridge, UK) overnight at 4°C. Biotinylated goat anti-rabbit IgG antibody (0.75 µg/mL, BA-1000, Vector Laboratories, Burlingame, CA) and Vectastain Elite ABC kit (PK-6100, Vector laboratories, Burlingame, CA) were used for visualization. Sections were counterstained with Mayer's hematoxylin, examined at 100X (Nikon Eclipse E800 microscope; Nikon, Tokyo, Japan) and imaged with a Nikon DS-5Mc camera, using Nikon DS-U1 control unit and NIS-Elements v3.22.

Whole mounts were permeabilized with 0.5% Triton X-100 in PBS and blocked for 2h with 2% BSA in 0.2% Triton X-100 in PBS prior incubation with anti-NFATc3 (sc-8321, 0.2 µg/mL, Santa Cruz Biotechnology) or anti- cluster of differentiation 31 (CD31; sc-1506, 0.8 µg/mL, Santa Cruz Biotechnology) for 48 hours at room temperature, followed by incubation Cy5 anti-rabbit IgG (3 µg/mL; Jackson Immuno Research). Nuclei were stained with SYTOX green. Whole mounts and sections were examined at 20X and 63X, respectively using a Zeiss LSM 5 laser scanning confocal microscope. Specificity of immune staining was confirmed by the absence of staining when primary antibodies were omitted from the protocol. NFATc3 nuclear accumulation in skin microvessels was quantified as previously described. [2, 6, 7] Briefly, for scoring of NFATc3-positive nuclei in vessels, multiple fields for each skin section were analyzed under blinded conditions. A cell was considered positive if co-localization was observed in the nucleus, whereas a cell was considered negative if no

co-localization was visualized. A minimum of 100 cells per animal were inspected. For visualization of co-localized image regions or double tagged regions (red: NFATc3 tagged with Cy5 and green: nuclear regions tagged with SYTOX Green), the crosshair function of the LSM program was used. This tool leads to the distribution of all image pixels over 4 quadrants in a scattergram according to their intensity levels, with the background pixels sorted into the bottom left quadrant, the single-tagged pixels (either red or green) into the upper left and bottom right quadrants, and the pixels having an intensity above the background in both channels (i.e., co-localized pixels) represented by the upper right quadrant. The image pixels corresponding to the upper right quadrant are then color-coded white in the original image to allow fast identification of co-localized areas.

Skin organ culture and enzymatic dissociation of dermis and epidermis

Two days after removing the fur by shaving and with depilatory cream (Veet® Reckitt-Benckiser), skin from the flank of WT/NFAT-luc mice was dissected out, cleaned from fat and muscle and cut into pieces (~2-3 x 2-3 mm). These were cultured with or without A-285222 (1 μmol/L) in DMEM (Dulbecco's modified minimal essential medium; F0405; Biochrom GmbH, Berlin, Germany) supplemented with 5 mmol/L glucose, 200 μg/mL BSA, 50 U/mL penicillin and 50 μg/mL streptomycin, at 37°C for various time-points up to 48 hours as indicated in the figure legends, according to a protocol that has been shown to preserve human and rodent skin structure and function for extended periods of time. [8, 9] After organ culture, the skin was frozen in liquid nitrogen and stored at -80°C until enzymatic dissociation of dermis and epidermis according to a previously described protocol. [10, 11] Briefly, whole skin was incubated with dispase II (5 μg/mL; Gibco Life Technology, Stockholm, Sweden) for 45 minutes at 37°C, after which fractions were manually dissected under a light microscope. In order to test for potential effects of the enzymatic dissociation on protein quantities or integrity, the method was compared to manual microdissection without prior enzymatic incubation and no differences were observed (data not shown). For western blot experiments to assess eNOS and p-eNOS (see below), microdissection only was used given that the method proved to be more time efficient when processing large number of samples.

RNA isolation, quantitative RT-PCR and absolute copy number of NFAT isoforms

Total RNA was isolated from skin (whole skin and dissociated dermis and epidermis as explained above) and thymus using TRI Reagent (Sigma Aldrich, Stockholm, Sweden) as previously described [12]. cDNA was synthesized with RevertAid First Strand cDNA kit, (Thermo Fisher Scientific, Stockholm, Sweden) and amplified using TaqMan gene expression assays for mouse eNOS Mm00435217_m1, a custom designed assay for luciferase mRNA (forward primer AACTGCCTGCGTCAGATTCTC, reverse primer AGTATCCGGAATGATTTGATTGC, FAM-labelled probe ATGCCAGGGATCCTA), OPN (Mm00436737_mL) and IL-6 (Mm00446190_ml) on a Viia7 instrument (Applied Biosystems, Carlsbad, CA). Target gene expression was normalized to HPRT Mm00446968_m1 and cyclophilin B Mm00478295_m1 and relative mRNA quantity was calculated using the comparative threshold method ($\Delta\Delta C_t$). All reactions were performed in triplicates.

For the absolute quantification of NFAT isoform expression, thymus cDNA was amplified using TaqMan gene expression assays for NFATc1 Mm00479445_m1; NFATc2 Mm01240679_m1; NFATc3 Mm01249200_m1; NFATc4 Mm00452375_m1 and β-actin Mm00607939_s1. PCR fragments were isolated using NucleoSpin Gel and PCR Clean-up kit (Macherey-Nagel, Düren, Germany) and concentrations were determined spectrophotometrically (NanoDrop ND-1000; NanoDrop Technologies, Wilmington, DE). The number of copies per μl for each NFAT isoform and for β-actin was calculated using the formula [X * 6.022×10^{23} molecules/mole] / [N * 660 g/mole] where X is the concentration of isolated PCR fragments in g/μl and N is the length of the PCR product in base pairs. [13] Ten-fold serial dilutions from 10^9 to 10 copies per μl were prepared and amplified in triplicates to generate absolute standard curves for each isoform, from where copy numbers for dermis

and epidermis samples, expressed per μg of total RNA input, were determined by reading off their threshold cycle (Ct) values after amplification in triplicates.

Western Blot

Whole skin, dermis and epidermis were homogenized using a glass tissue grinder (Wheaton, Fischer Scientific, Sweden) and proteins were extracted using TRI Reagent (Sigma Aldrich, Stockholm, Sweden) according to the manufacturer's instructions. Protein concentration was determined using EZQ protein quantification kit (Molecular Probes, Invitrogen, Paisley, UK) and an equal amount of protein was loaded in 4-15% Mini Protean TGX Stain-free gels (Bio-Rad Laboratories, Sundbyberg, Sweden) and transferred to 0.2 μm PVDF membranes using Trans-Blot turbo (Bio-Rad Laboratories, Sundbyberg, Sweden). Membranes were probed overnight at 4°C with primary antibodies against CD31 (sc-1506, 1 μg/mL, Santa Cruz Biotechnology, Santa Cruz, CA) and α-tubulin (A01410, 0.1 μg/mL, GenScript Corporation, Piscataway, NJ) with horseradish peroxidase-conjugated secondary antibodies (1:10,000; Cell Signal Technology, Danvers, MA). Labeling was detected by chemiluminescence (Supersignal West Dura, Thermo Scientific, MA).

For quantification of eNOS and p-eNOS, dermis was processed using a OMNI TH tissue homogenizer (OMNI International, Kennesaw GA, US) and proteins were extracted using TRI Reagent as described above. Proteins were separated on 4-15% TGX Stain-free gels and transferred to 0.45 μm low-fluorescence PVDF membranes. Membranes were then imaged for total protein quantification and probed overnight at 4°C with primary antibodies against eNOS (sc-376751, 0.4 μg/mL Santa Cruz Biotechnology, Santa Cruz, CA) or p-eNOS (Ser1177, sc-81510, 0.1 μg/mL Santa Cruz Biotechnology, Santa Cruz, CA). Data quantification was performed using Image Lab Software (Life Science Research, Bio-Rad Laboratories, Sundbyberg, Sweden). Signal intensity was normalized to total protein measured in the membrane after transfer. For each animal, dermis from 3-4 pieces of skin, each of~2-3 x 2-3 mm, were pooled to generate a data point.

Plasma cytokines, endothelial activation markers and total NO

Plasma levels of cytokines [interleukin (IL)-1α, IL-6, IL-10 and osteopontin (OPN)] and endothelial activation markers [soluble intercellular adhesion molecule 1 (sICAM), E-selectin, endothelin-1 (Et-1)] were measured in blood samples taken from the tail vein before and after A-285222 treatment (Pre, Post-1 and Post-2) Plasma cytokine levels were measured using the Bio-Plex™ multiplex ELISA system (Bio-Rad Laboratories, Hertfordshire, UK) and sICAM, E-selectin, Et-1and OPN were measured using Quantikine Colorimetric sandwich ELISA assays (R&D Systems, Bio-Techne Ltd, Abingdon, UK). Total NO related species (nitrite, nitrate, nitrosothiols) were measured 4 weeks after treatment with A-285222 (Post-2) using a gas phase chemiluminescence reaction of NO with ozone using Sievers nitric oxide analyzer (NOA) model 280i (Analytix, Bodon, UK).

Blood pressure

Blood pressure was assessed in conscious mice four weeks after treatment with A-285222 (Post-2) using a computerized tail-cuff non-invasive blood pressure system (CODA; Kent Scientific, Connecticut, USA). Before measurements were initiated, mice were adapted to the apparatus for at least 5 days.

Urinary albumin measurements

Urine was collected from the bladder at termination. Urinary albumin excretion was measured using an indirect competitive ELISA (Albuwell M, Exocell, Philadelphia, PA) and urinary creatinine concentration was measured using a picric acid assay (Creatinine Companion; Exocell); all according to the manufacturers' instructions.

Chemicals

A-285222 was kindly provided by Abbott Laboratories (Abbott Park, IL). All other chemicals were from Sigma Aldrich unless otherwise specified.

Statistics

Results are expressed as means ± SEM unless otherwise specified. Statistical significance was determined using Student's t-test and one or two-way ANOVA followed by Dunnett's multiple comparisons or Bonferroni *post hoc* tests. For survival analysis Kaplan-Meier curves were generated from data compiled throughout the study and Mantel-Cox log-rank test performed to compare survival between groups. Statistical analyses were performed using SPSS version 14.1 or GraphPad software (Prism 6.0 and 7.0).

References

1. Nilsson J, Nilsson LM, Chen Y-W, Molkentin JD, Erlinge D, Gomez MF. High glucose activates nuclear factor of activated t cells in native vascular smooth muscle. *Arteriosclerosis, thrombosis, and vascular biology*. 2006;26:794-800
2. Nilsson LM, Sun ZW, Nilsson J, Nordstrom I, Chen YW, Molkentin JD, Wide-Swensson D, Hellstrand P, Lydrup ML, Gomez MF. Novel blocker of nfat activation inhibits il-6 production in human myometrial arteries and reduces vascular smooth muscle cell proliferation. *Am J Physiol Cell Physiol*. 2007;292:C1167-1178
3. Wilkins BJ, Dai YS, Bueno OF, Parsons SA, Xu J, Plank DM, Jones F, Kimball TR, Molkentin JD. Calcineurin/nfat coupling participates in pathological, but not physiological, cardiac hypertrophy. *Circulation research*. 2004;94:110-118
4. Belch JJ, Akbar N, Alapati V, Petrie J, Arthur S, Khan F. Longitudinal assessment of endothelial function in the microvasculature of mice in-vivo. *Microvascular research*. 2013;85:86-92
5. Akbar N, Nanda S, Belch J, Cohen P, Khan F. An important role for a20-binding inhibitor of nuclear factor-kb-1 (abin1) in inflammation-mediated endothelial dysfunction: An in vivo study in abin1 (d485n) mice. *Arthritis research & therapy*. 2015;17:22
6. Stevenson AS, Gomez MF, Hill-Eubanks DC, Nelson MT. Nfat4 movement in native smooth muscle. A role for differential ca(2+) signaling. *The Journal of biological chemistry*. 2001;276:15018-15024
7. Gomez MF, Stevenson AS, Bonev AD, Hill-Eubanks DC, Nelson MT. Opposing actions of inositol 1,4,5-trisphosphate and ryanodine receptors on nuclear factor of activated t-cells regulation in smooth muscle. *The Journal of biological chemistry*. 2002;277:37756-37764
8. Varani J. Preservation of human skin structure and function in organ culture. *Histology and histopathology*. 1998;13:775-783
9. Varani J, Perone P, Merfert MG, Moon SE, Larkin D, Stevens MJ. All-trans retinoic acid improves structure and function of diabetic rat skin in organ culture. *Diabetes*. 2002;51:3510-3516
10. Hybbinette S, Bostrom M, Lindberg K. Enzymatic dissociation of keratinocytes from human skin biopsies for in vitro cell propagation. *Experimental dermatology*. 1999;8:30-38
11. Stenn KS, Link R, Moellmann G, Madri J, Kuklinska E. Dispase, a neutral protease from bacillus polymyxa, is a powerful fibronectinase and type iv collagenase. *The Journal of investigative dermatology*. 1989;93:287-290
12. Zetterqvist AV, Berglund LM, Blanco F, Garcia-Vaz E, Wigren M, Duner P, Andersson AM, To F, Spegel P, Nilsson J, Bengtsson E, Gomez MF. Inhibition of nuclear factor of activated t-cells (nfat) suppresses accelerated atherosclerosis in diabetic mice. *PloS one*. 2013;8:e65020

13. Dhanasekaran S, Doherty TM, Kenneth J, Group TBTS. Comparison of different standards for real-time pcr-based absolute quantification. *Journal of immunological methods*. 2010;354:34-39